

# The Origins and Evolutionary Status of B Stars Found Far From the Galactic Plane II: Kinematics and Full Sample Analysis<sup>1</sup>

J. C. Martin<sup>2</sup>

*Case Western Reserve University Astronomy Department  
Cleveland, OH 44106*

`jmartin@astro.umn.edu`

## ABSTRACT

This paper continues the analysis of faint high latitude B stars from Martin (2004). Here we analyze the kinematics of the stars and combine them with the abundance information from the first paper to classify each one. The sample contains 31 Population I runaways, fifteen old evolved stars (including five BHB stars, three post-HB stars, a pulsating helium dwarf, and six stars of ambiguous classification), one F-dwarf, and two stars which do not easily fit in one of the other categories. No star in the sample unambiguously shows the characteristics of a young massive star formed in situ in the halo. The two unclassified stars are probably extreme Population I runaways. The low binary frequency and rotational velocity distribution of the Population I runaways imply that most were ejected from dense star clusters by DES (dynamic ejection scenario). However we remain puzzled by the lack of runaway Be stars. We also confirm that PB 166 and HIP 41979 are both nearby solar-metallicity BHB stars.

*Subject headings:* stars: abundances, stars:early-type, stars:evolution, stars:kinematics, stars: rotation, stars: Be

---

<sup>2</sup>Currently at University of Minnesota, School of Physics and Astronomy, Minneapolis, MN 55455

<sup>1</sup>Based on observations made at the 2.1-m Otto Struve Telescope of McDonald Observatory operated by the University of Texas at Austin

## 1. Introduction

One in three faint high galactic latitude B stars have spectral characteristics which are indistinguishable from nearby Population I B stars (Greenstein & Sargent 1974). Assuming that these are main sequence stars, their faint apparent magnitudes imply that they are several kiloparsecs above the galactic plane. These stars most likely fall into one of three categories:

1. “Normal” massive Population I stars ejected from the galactic disk,
2. Misidentified older evolved stars (i.e. blue horizontal branch (BHB), post-HB, AGB-manqué, or post asymptotic giant branch (PAGB) stars), or
3. Young massive stars formed in situ in the galactic halo.

Paper I (Martin 2004) analyzed the compositions of forty apparently normal main sequence B stars, that are mostly 0.5 to 2 kiloparsecs from the galactic plane, to determine to which of those three categories each belonged. The abundances revealed: twenty two with Population I abundances, nine with post-main sequence evolution, eight which could only be characterized as metal poor, and one that was unclassifiable. Several of those stars which did not appear to have normal disk-like abundances also had other distinguishing characteristics including variability and/or unique emission features. Combining that data with the abundances, we arrived at the following preliminary classifications:

- Runaway Population I stars: 21 stars are indistinguishable from nearby Population I B stars, implying that they had been ejected from the disk.
- Old evolved stars: 10 stars have abundance patterns and characteristics which are expected in BHB, post-HB, AGB-manqué, PAGB, or PPN stars (e.g. enhancement or depletion of specific elements by nuclear processing, atomic diffusion, and/or depletion of refractory elements by dust grain formation).
- F dwarf: AG +03 2773 appears to have been misclassified and is probably an early type F dwarf
- Unknown: 17 stars have insufficient or conflicting information and cannot be categorized as runaway Population I stars or old evolved stars. This category contains any stars that may have formed in situ in the halo.

This paper analyzes the kinematics of each star and combines those results with Paper I to reclassify each star as a Population I runaway, an old evolved star, or a young massive star formed in situ in the halo. Refer to Paper I for a detailed description of the stellar samples and the spectra. In Section 2 we review the expected kinematics for each of these stellar populations along with numerical simulations that predict the kinematic distribution of runaway stars. In Section 3 we discuss the raw data the methods used to calculate the space velocities and in Section 4 we analyze those space velocities. In Section 5 we combine the kinematic data with the results from Paper I to make final classifications of each star and discuss the overall breakdown of the sample in Section 6. Finally, in Sections 7 and 8 we analyze the properties of the stars within each category to infer more about the origins and characteristics of each stellar population.

## 2. Background & Theory

### 2.1. An Overview of the Milky Way

The velocities of the stars in three dimensions are calculated in the galactocentric cylindrical coordinate system ( $V_\pi, V_\theta, V_z$ ). In this frame of reference,  $V_\pi$  is radial motion relative to the galactic center with positive  $V_\pi$  directed away from the center of the Milky Way.  $V_\theta$  is the rotational velocity component, orthogonal to  $V_\pi$  in the galactic plane and positive in the direction of galactic rotation.  $V_z$  is velocity perpendicular to the galactic plane (parallel to the spin axis of the galaxy), with positive  $V_z$  towards the North Galactic Pole (NGP). In this system, the Sun is 8 kpc from galactic center and moving with a velocity of  $(V_\pi, V_\theta, V_z) = (-9 \text{ km s}^{-1}, 232 \text{ km s}^{-1}, 7 \text{ km s}^{-1})$ , (the solar motion is the sum of the motion of the Local Standard of Rest (LSR,  $V_\theta = 220 \text{ km s}^{-1}$ ) and the Sun’s own peculiar motion (Mihalas & Binney 1981)).

The Milky Way has three main kinematic components: the bulge/bar, the disk, and the halo. None of the stars in this sample should be associated with the bulge or bar since the influence of that population is confined to within several kiloparsecs of the galactic center. Any of the stars in the sample could be members of the halo but only those within about a kiloparsec from the galactic plane could be considered part of the thick disk. Table 1 shows the generally accepted velocity distributions of the thin disk, thick disk, and halo populations. The disk populations are characterized by a strong rotational component ( $V_\theta$ ) with relatively small velocity dispersions. The halo population, by contrast, has much larger isotropic velocity dispersions, with no strong signature of rotation. As a result, halo stars tend to have significantly larger  $V_\pi$  and  $V_z$  than most disk stars.

The three categories of faint high latitude B stars belong to separate galactic populations, each with their own kinematic properties and signature. Massive stars that formed in situ in the halo should have halo-like kinematics which are similar to the high-velocity clouds they formed in. Low mass old evolved stars can belong to either the halo or thick disk populations. Runaway Population I stars occupy the same volume as the halo but retain a strong rotational component to their velocity. This makes them a kinematically unique population that combines the characteristics of both the disk and the halo.

## 2.2. Runaway Population I Stars

There are two mechanisms that have been proposed to launch Population I B stars from the galactic disk: the binary supernova scenario (BSS; also called the Blaauw Hypothesis) and the dynamic ejection scenario (DES). The binary supernova scenario (BSS) was first proposed by Zwicky (1957) and later formalized by Blaauw (1961). In this scenario the secondary star in a binary is ejected when the primary goes supernova and the system loses enough mass to become unbound. Stars launched by BSS are ejected with space velocities comparable to their original orbital velocity (up to  $200 \text{ km s}^{-1}$ ; Portegies Zwart (2000)). Monte Carlo simulations by Portegies Zwart (2000) predict that in 20% – 40% of BSS ejections the neutron star produced in the supernova will remain bound to the runaway with an orbital period of several hundred days.

Poveda, Ruiz, & Allen (1967) describe an alternate mechanism where stars receive a velocity kick from close dynamic interactions between pairs of binaries or single stars and binaries. This scenario, known as the dynamic ejection scenario (DES), is probably most efficient in densely populated star clusters or star forming regions. Simulations by Leonard & Duncan (1990); Leonard (1991); Iben & Tutukov (1997) show that most DES encounters should produce one or more single runaway stars with velocities up to  $300 \text{ km s}^{-1}$ .

### 2.2.1. Probing the Galactic Potential With Runaways

As demonstrated in Appendix A, the makeup of the galactic potential influences the trajectories and flight times of the stars in the sample. Theoretically, the problem can be reversed to constrain the galactic potential using the fact that no runaway star has a flight time which exceeds its main sequence lifetime. However, in practice the uncertainty in the main sequence lifetimes is too large to constrain the potential in any meaningful way. We are also limited by the degree to which components of the potential influence individual stars.

The flight times of these stars are mostly insensitive to the bulge component or changes in the scale length of the disk. Then, only stars within about 1.5 kpc of the plane have any significant sensitivity to changes in the disk mass surface density. Therefore, small number statistics, lack of sensitivity to changes in the potential, and uncertainty in the main sequence lifetimes conspire to make runaway B stars unsuitable as tracers for placing meaningful constraints on the galactic potential.

### 2.2.2. Runaway Sample Bias

If we assume main sequence luminosities and distances for all the stars in the sample, then over 70% of them are between 0.5 kpc and 2 kpc from the galactic plane (Table 5, Figure 1). This de facto bias translates directly into a kinematic selection effect which prevents us from using the runaways to probe the range of ejection velocities imparted by BSS or DES. However, it is useful to us because it gives the runaways a distinct kinematic signature in their  $V_\pi$  and  $V_\theta$  space velocities (see Section 2.2.3).

Runaways launched from the galactic disk follow a ballistic trajectory. As a result, they spend more time near the apex of their trajectory than traveling to or from that point. Therefore, most runaways will be observed near to their maximum displacement from the galactic plane. This is why most of the runaways in our sample have relatively small  $V_z$  velocities (Table 5) and are found near the theoretical apex of their orbits (Figure 1). The maximum displacement from the plane is directly proportional to the kick which a runaway receives in the  $V_z$  direction ( $Z_{ej}$ ) so that a volume limited sample will contain mostly stars with a given range of  $Z_{ej}$ . The parameters of this sample make it heavily biased in favor of stars with  $Z_{ej}$  between  $50 \text{ km s}^{-1}$  and  $125 \text{ km s}^{-1}$  (assuming that the galactic potential matches the one in Appendix A).

The relationship between  $Z_{ej}$  and the total ejection velocity ( $V_{ej}$ ) is more complex. We computed the sample’s bias in terms of  $V_{ej}$  by Monte Carlo simulation using the galactic potential model in Appendix A and the following assumptions that model the parameters of our sample:

- The stars fall between 0.5 and 2 kpc from the galactic plane
- Runaways are observed near the apex of their trajectory, and
- There is no preferred direction for the orientation of  $V_{ej}$  vector in space (all angles are equally likely). In other words,  $Z_{ej}/V_{ej}$  is equally likely to have any value between zero and one.

The results of the simulation are not sensitive to the upper bound of the first assumption. Stars reaching a maximum height of 3 kpc or 4 kpc have  $Z_{ej}$ s which are  $41 \text{ km s}^{-1}$  and  $79 \text{ km s}^{-1}$  faster than those reaching 2 kpc (Figure 1). This has only a slight affect on the high velocity tail of the distribution. The second assumption is merely, as explained above, an application of Kepler’s Second Law. Figure 1 confirms that the runaways in the sample are found near the apex of their trajectories.

The computed bias in terms of total ejection velocity is presented in Figure 2 along with the distribution of ejection velocities for the runaways in our sample (see Section 3.6). The sample bias is the dominate factor shaping the distribution of ejection velocities. A sharp cutoff occurs between  $50 \text{ km s}^{-1}$  and  $100 \text{ km s}^{-1}$  because stars ejected with  $V_{ej}$  smaller than  $50 \text{ km s}^{-1}$  are unable to reach a height of 0.5 kpc from the plane even if all their velocity is directed in the  $V_z$  direction. Given this overwhelming bias, we must conclude that this sample can not provide any useful information with respect to the distribution of  $Z_{ej}$  or  $V_{ej}$ . Future studies which intend to measure the distribution of ejection velocities must sample many more runaway stars over a wider range of distances (i.e. 0.1 to 5 kpc) from the galactic plane.

### 2.2.3. *Expected Runaway Velocities in the $V_\pi$ versus $V_\theta$ Plane*

While the sample bias is crippling with respect to the distribution of  $Z_{ej}$  and  $V_{ej}$ , it can be used to identify the runaways in the sample by their space velocities. The remainder of  $V_{ej}$  that is not in  $Z_{ej}$  is distributed between the  $V_\pi$  and  $V_\theta$  components. Because the runaways are ejected from the thin disk population, their  $V_\pi$  and  $V_\theta$  velocities will be the sum of their ejection velocities and the rotation of the rest frame in the galactic disk that they were launched from. As a result, a plot of  $V_\pi$  versus  $V_\theta$  for runaway stars should be centered on the LSR ( $V_\pi = 0 \text{ km s}^{-1}$ ;  $V_\theta = 220 \text{ km s}^{-1}$ ) and kinematically heated to a degree directly influenced by the distribution of ejection velocities present in the sample. This distribution contrasts with halo stars, which should have no strong  $V_\theta$  component and larger  $V_\pi$  components on average.

We ran a Monte Carlo simulation of  $V_\pi$  and  $V_\theta$  velocities of runaway stars using the galactic potential model described in Appendix A and the following parameters:

1. The runaways in the sample originate in the galactic thin disk within 1.0 kpc of the Sun. (see below)
2. The maximum total ejection velocity of a runaway is  $400 \text{ km s}^{-1}$ . (see Iben & Tutukov (1997) and Portegies Zwart (2000))

3. The portion of the total ejection velocity for a runaway which is not in  $Z_{ej}$  is randomly distributed between the  $V_\pi$  and  $V_\theta$  components, with the initial pre-ejection velocity equal to the LSR ( $V_\pi = 0 \text{ km s}^{-1}$ ;  $V_\theta = 220 \text{ km s}^{-1}$ ).
4. Runaways are observed at the apex of their trajectories. (Kepler’s Second Law)
5. Runaways included in the simulation have trajectories with maximum heights of 0.5 kpc to 2 kpc from the galactic plane. (see Section 2.2.2)
6. The position of a runaway at its maximum displacement from the galactic plane is at least 30 degrees above the galactic plane as viewed from the Sun. (see the sample selection criteria in Paper I)

The results of the simulation are presented in Figure 3. Note that nearly all the runaway stars fall within  $100 \text{ km s}^{-1}$  of the LSR. The fuzzy diagonal structure to the lower left of the LSR can be explained by the behavior of a particle in a Keplarian potential. An orbiting object which receives a kick slowing its orbital velocity (decreased  $V_\theta$ ) will move radially inward (negative  $V_\pi$ ) while an object receiving a kick increasing its orbital velocity (increased  $V_\theta$ ) will move radially outward (positive  $V_\pi$ ). This creates a noticeable diagonal pattern in the velocity field. While the galactic potential is not Keplarian, it is reasonably approximated as such for the purpose of this argument.

The second assumption further negates the significance of the upper bound in the fifth assumption. If more of a star’s  $V_{ej}$  is partitioned into  $Z_{ej}$  (to make it go further from the plane) then there is less velocity to distribute into the  $V_\theta$  and  $V_\pi$  velocity components. This makes a *tighter* and more centrally concentrated velocity distribution about the LSR in the  $V_\theta$  versus  $V_\pi$  plane.

The first assumption in the simulation also has little effect on the outcome. If we assume that the runaways have originated in or near discrete local star forming regions instead, the general size and shape of the velocity distribution remains the same (Figure 4). There are some subtle differences between the distributions which are dependent on the distance and location of each star forming region relative to the Sun. However, these differences are small in relation to the typical observational errors associated with the stellar velocities measured in this study and it took thousands of points in the Monte Carlo simulation to make the differences between these patterns noticeable.

### 3. The Data & Calculations

#### 3.1. Full Space Velocities

The full space velocities of the stars are computed using the algorithm of Eggen (1961). The input parameters to this algorithm include: distance, proper motion, and radial velocity. The errors in the velocities were estimated from the errors of the input parameters using a Monte Carlo technique. The largest contribution to the errors is from the proper motions because they are multiplied by the distance and usually have errors that are a significant fraction of their value. Uncertainty in the other factors also contributes to the over-all errors but to a lesser degree.

For diagnostic purposes our first assessment of each star’s velocity is made assuming that it is a main sequence star. In doing so, we purposefully over estimated the distances and space velocities of the less intrinsically luminous evolved stars in the sample. That fact is used to distinguish them from the Population I runaways and in Section 8.1 we will revisit the velocities of the less massive and luminous stars using more appropriate assumptions.

#### 3.2. Proper Motions

Every star in the study has proper motions from the Hipparcos Catalog (HIP) (Perryman & ESA 1997), the Tycho-2 Catalog (Høg et al. 2000), and at least one other catalog including: the ACT (Urban et al. 1997), the Carlsberg Meridian Catalogs (CMC) (Fabricius 1993), and the First U.S. Naval Observatory CCD Astrograph Catalog (UCAC1) (Zacharias et al. 2000). Three or more independent proper motion measures for each star were combined by weighted average as described in Martin & Morrison (1998). In most cases, the errors of the average proper motions are a factor of 1.5 to 2.0 smaller than the errors in the Hipparcos catalog (Table 2).

#### 3.3. Main Sequence Distances

As noted above, the distances to the stars in the sample of study are first determined by photometric parallax assuming that all the stars have main sequence luminosities. Blue horizontal branch (BHB) stars are significantly less luminous than main sequence B stars with the same effective temperature. Therefore the distance to a BHB star will be overestimated if the intrinsic luminosity of a main sequence star is used to calculate its photometric parallax. An overestimated distance will in turn inflate the space velocity for a star so that a sub-



luminous star which is a member of the thick or thin disk population may kinematically appear to be a member of the halo. In the most extreme cases, an overestimated distance can even result in velocities that appear to exceed the galaxy’s escape velocity in the Solar Neighborhood (at least  $500 \text{ km s}^{-1}$ ; Carney et al. (1988)).

Due to their sub-luminous nature, BHB stars in the sample are not several kiloparsecs above the plane, but actually only a few hundred parsecs away. Assigning these stars main sequence distances will help to kinematically separate them from the rest of the sample. We will revisit them in Section 8.1 to evaluate their “true” space velocities with more reasonable assumptions about their intrinsic luminosities and distances.

Absolute Johnson V magnitudes were calculated for each star from the bolometric magnitudes and bolometric corrections. The bolometric magnitudes were determined by matching the effective temperature, surface gravity, and metallicity of each star the models of Schaller et al. (1992). The bolometric corrections were interpolated using the same parameters from a grid of models computed with ATLAS12<sup>2</sup> (Kurucz 1996).

We compared the absolute magnitudes from this method with those calculated by the method of Cramer (1999) for the stars in our sample with Geneva Photometry (see Paper I). The Cramer (1999) relation was calibrated using Hipparcos parallaxes to obtain the distances and intrinsic luminosities of stars fitted as a function of the Geneva reddening free X and Y color indices (Cramer & Maeder 1979). There are fewer stars with Hipparcos parallaxes to calibrate the hot end of the relation ( $T_{eff} \geq 30000 \text{ K}$ ) so one must be cautious applying this relation in that regime. This method is also only valid for stars with effective temperatures hotter than 11000 K because it uses the X and Y indices.

There is a trend in the difference between the absolute magnitudes calculated by our method and the method of Cramer with respect to the Geneva Y index (Figure 5). The outliers from the main group in that diagram are stars which are obviously not main sequence stars that lie outside the normal regime of the Cramer relation. The Geneva Y index is a measure of a B star’s separation from the main sequence (Cramer & Maeder 1979). Therefore the trend in Y suggests that the Cramer relation does not completely account for changes in brightness as a star evolves away from the zero-age main sequence (ZAMS). The Cramer relation was developed from the limited number of B stars with measurable Hipparcos parallaxes so it is afflicted by small number statistics and strongly biases by galactic structures such as Gould’s Belt<sup>3</sup>. Many of the stars in this sample are at least several tens of

---

<sup>2</sup>Grids computed by ATLAS12 using up to date opacities and atomic data are available online from <http://kurucz.harvard.edu/grids>.

<sup>3</sup>Gould’s Belt (Stothers & Frogel 1974) is a structure in the solar neighborhood roughly 1 kpc in diameter

Myr evolved from the ZAMS (as evidenced from their flight times, see Section 3.6) so that evolution has had a significant effect on their absolute luminosity.

The Cramer relation has an internal formal error of 0.44 mag which corresponds roughly to a factor of 20% in distance. Considering our sources of error, those of Schaller et al. (1992), and the random spread in our comparison with the Cramer (1999) relation, the photometric distances are assigned a  $\pm 30\%$  error (0.57 magnitudes).

HD 138503 is an eclipsing binary composed of two main sequence B stars that was analyzed by Martin (2003). From that work, a distance of 2.4 kpc is adopted with an error of  $\pm 30\%$ . This distance is significantly greater than the distance derived from our method described above ( $1.3 \pm 0.4$  kpc). However this discrepancy is explained by HD 138503’s binary nature which makes the pair more luminous together than a single star at the same distance.

In Paper I, we showed that AG +03 2773 is probably a rapidly rotating F dwarf. To calculate its distance we assumed an effective temperature of 7000 K with a surface gravity of 4.0 and roughly solar composition. This yielded a distance of 400 pc which is consistent with its Hipparcos parallax ( $0.23 \pm 2.05$ ).

### 3.4. Radial Velocities

Radial velocities were measured for forty (41) of the stars in the sample. The high resolution ( $R=60000$ ) spectra taken for the abundance analysis were used to measure the radial velocities of the stars from the Doppler shift of their photospheric absorption lines. (For a detailed description of the spectra see Section 2.1 in Paper I.) The resolution of the spectrograph (one resolution unit equals two pixels) is about  $2 \text{ km s}^{-1}$  but the FFT interpolates four points to each pixel allowing an even higher precision to be achieved. The precision of the radial velocities is primarily influenced by our capability to determine the line center. This becomes more difficult with an increase in rotational broadening.

The process of measuring the wavelengths of line centers was interactive. Lines that appeared to be blended or had no clear minimum in the profile were excluded from the analysis. The line centers are defined by the minima in the line profiles in the continuum corrected FFT filtered data. High rotational broadening and low signal to noise sometimes drastically limited the number of lines that could be measured in a spectrum. In a three

---

that is composed of stars in a ring of OB associations that are all close to the same evolutionary age (Perrot & Grenier 2003).

desperate cases (HD 15910, HIP 12320, and HD 106929), where no other lines could be measured with confidence, only the hydrogen Balmer lines were used to determine the radial velocity of the star. Because the spectral orders have some wavelength overlap, several lines were measured on two adjacent spectral orders. Each of these were treated as independent measures when computing the average value. The average radial velocity for a spectral observation is calculated as a straight unweighted average of the values from each of the observed lines. Since the distribution of individual measurements is roughly Gaussian, the error of that average is estimated from the standard deviation of the measurements.

The IRAF procedure `noao.rv.rvcorrect` was used to transform the observed radial velocities into the heliocentric reference frame using the date and time at mid-exposure. For spectra that consisted of combined exposure sets from several nights, the correction factor was not significantly different for each exposure set and an average value was used.

Radial velocity standards from Fekel (1999) were used to verify the measured radial velocities. Table 3 shows that this method is able to accurately reproduce the radial velocities of the standard stars. There is good agreement between most of the radial velocities we measured (Table 2) and those published in the literature (Table 4). Later in Section 7.1 we will discuss if any of the discrepancies in Table 4 imply that some of these stars are binaries.

The radial velocities of ten stars were taken from the literature for the following reasons:

- No spectra were obtained for six stars in the sample.
- HD 140543 has irregularly shaped lines that proved difficult to measure with any confidence.
- The systemic velocity of BD +13 3224 could not be determined with any confidence because the lines were smeared (the exposures were too long compared to the very short period of this pulsating helium dwarf).
- HD 135569 is a long period binary so we relied on the analysis of Bolton & Thomson (1980) for the systemic velocity.
- The systematic radial velocity of eclipsing binary HD 13503 (IT Lib) was analyzed separately by Martin (2003).

### 3.5. Main Sequence Lifetimes

The projected main sequence lifetimes ( $T_{MS}$ ) for the stars in the sample were determined from their effective temperature, surface gravity, and metal content from the tables of Schaller

et al. (1992). If the metallicity of the star is not known, the longest main sequence lifetime for any metallicity is used. The results for each star are listed in Table 5. The error in the main sequence lifetime is difficult to estimate since stellar rotation and other mixing can affect the hydrogen burning lifetime of a massive star by as much as 30% (Heger & Langer 2000). Other processes (i.e. convection, overshooting, and semiconvection) are only roughly modeled and magnetic fields are completely ignored, affording significant additional uncertainty (Heger et al. 2000). Considering these factors and the uncertainty of converting the effective temperatures and metallicities to main sequence lifetimes, we have adopted an error of  $\pm 50\%$  for the estimated main sequence lifetimes. The error could be larger than this for the highest mass stars (shortest main sequence lifetimes).

### 3.6. Ejection Velocities and Flight Times

Initial ejection velocities perpendicular to the plane ( $Z_{ej}$ ) and travel times back to the disk ( $T_{flight}$ ) are computed from the full space velocities of each star (assuming main sequence distances) using a model of the galactic potential and an orbital integrator outlined in Appendix A and described in detail by Harding et al. (2001). Errors in  $Z_{ej}$  and  $T_{flight}$  were estimated from the errors in each star’s position and space velocity by Monte-Carlo simulation.

The time of flight for each star is measured from the star’s present position to  $Z = 0$  along its orbit in the galactic potential. Stars that are moving back toward the galactic plane are traced back through the apex of their orbit. It is reasonable to assume that each star began at  $Z=0$  since most star forming regions are found very close to the galactic plane. However, a few like the Orion complex are up to 100 pc from the galactic plane. In those cases the difference between the actual launch point and  $Z = 0$  has negligible effect on the flight times because the stars are moving with velocities on the order of hundreds of  $\text{km s}^{-1}$  when they are close to the plane and traverse 100 pc in less than 1 Myr (well within the margin of error). The flight times and  $Z_{ej}$  for the sample stars are given in Table 5.

## 4. Analysis of Space Velocities

Table 5 lists the spatial coordinates, full space velocities, main sequence lifetimes, ejection velocities, and flight times for the stars in the sample. A number of stars, PB 166, HD 218970, BD +33 2642, and HIP 1511 in particular, stand out as having unusually large velocities relative to the LSR. As noted in Section 3.3, these extreme velocities may be the

result of overestimating the distance to the star. The  $V_z$  for twenty two of the stars is under  $50 \text{ km s}^{-1}$ . As noted in Section 2.2.2, most runaways are observed near the apex of their trajectory so they should have  $V_z$  close to zero. Twelve (12) of the stars are actually moving back toward the galactic plane. If they are runaways, then these stars have already passed through the apex of their trajectory and are falling back toward the galactic disk.

#### 4.1. $V_\pi$ versus $V_\theta$

A plot of the  $V_\pi$  velocity versus  $V_\theta$  velocity for stars in the sample (Figure 6) shows that there is a significant clustering about the LSR ( $V_\theta = 220 \text{ km s}^{-1}$ ,  $V_\pi = 0 \text{ km s}^{-1}$ ) which is similar to the simulated runaway star distribution (Section 2.2.3, Figure 3). The region within  $100 \text{ km s}^{-1}$  of the LSR contains twenty four stars. These are the most likely runaway candidates in the sample. That is not to say that all twenty four stars in that region are definitely runaways but rather that this is one piece of evidence in favor of that classification. Likewise, some of the stars between  $100 \text{ km s}^{-1}$  and  $150 \text{ km s}^{-1}$  of the LSR are not completely excluded from being runaways but stars more than  $150 \text{ km s}^{-1}$  from the LSR are most likely not runaways.

#### 4.2. Main Sequence Lifetime versus Travel Time

Figure 7 compares the estimated main sequence lifetime to the calculated flight time for each star in the sample (assuming main sequence distances). Between the dotted lines the main sequence lifetime of a star is within  $\pm 50\%$  of the flight time (the estimated error, see Section 3.5). These lines divide the diagram into three regions: stars with flight times significantly longer than their project main sequence lifetimes (upper left), stars with flight times about equal to their main sequence lifetimes (between the lines), and stars with flight times which are definitely shorter than their main sequence lifetimes (lower right).

The upper left corner of the diagram contains stars that could have formed in situ in the halo or sub-luminous stars whose distances, velocities, and flight times have been overestimated. Only one star is from our sample is found in this part of the diagram: HD 140543. In that case it is possible that the error in the main sequence lifetime is greater than 50% so that its lifetime and travel time could be consistent. It is uncertain if there is any conflict between the flight times and hydrogen burning life times of the fifteen stars which fall between the dotted lines. The remaining thirty three stars to the right of the dotted lines could easily have traveled from the disk to their present location in their main sequence

lifetimes.

For comparison, we have highlighted the most likely runaway stars from Figure 6 (stars within  $100 \text{ km s}^{-1}$  of the LSR). All but HD 140543 fall between or to the right of the dotted lines, confirming that they are most likely stars which have been ejected from the galactic disk.

## 5. Kinematic Scoring and Classification

A four point scale is used to assign a kinematic score to each star in the sample (Table 6). The points are assigned to each star based on its velocity in the  $V_\pi$  versus  $V_\theta$  plane assuming main sequence distances (Figure 6) and a comparison between its flight time and main sequence lifetime (Figure 7) as follows:

- One point is awarded to each star within  $150 \text{ km s}^{-1}$  of the LSR in the  $V_\pi$  versus  $V_\theta$  plane.
- An additional point is awarded if the star is less than  $100 \text{ km s}^{-1}$  from the LSR in the  $V_\pi$  versus  $V_\theta$  plane.
- One point is awarded to each star in Figure 7 with a main sequence lifetime which is within 50% of their flight time (stars between the dotted lines).
- Two points are awarded to each star with a main sequence lifetime at least 50% greater than their flight time (stars to the right of all dotted lines).

In this scheme, a cumulative score of four represents a star with kinematics that are completely consistent with a runaway from the disk, while a score of zero denotes a star that is probably not a runaway. A high score does not ensure that a star is a runaway but a lower score lessens the likelihood that it was ejected from the disk.

### 5.1. Sample Breakdown and Classification

Table 6 combines the kinematic results from the preceding section with the abundance and spectral flux information from Paper I. These data are used to classify each star as a runaway Population I star, an old evolved star, or a massive young star formed in situ in the halo. While all the data are considered, the abundances are given more weight than

the other factors because we have a higher degree of confidence in those results. A question mark (?) after the classification denotes some uncertainty due to missing or conflicting data.

Two stars are labeled “unknown” (U) because they have kinematics that are somewhat inconsistent with Population I runaways but no other conclusive evidence as to their nature (see Section 5.3). Also recall from Paper I that AG +03 2773 is probably a misclassified F Dwarf. The remaining 46 stars can be conclusively sorted as either old evolved stars (15 stars) or Population I runaways (31 stars). *No star in this sample unambiguously shows the characteristics of a young massive star which formed in situ in the galactic halo.*

## 5.2. Breakdown of Old Evolved Stars

The stars classified as old evolved stars can be further sub-divided into BHB and post-HB stars. For the purpose of this study, a post-HB star is any star that has evolved past the horizontal branch. These include PAGB, AGB-manqué, and PPN (proto-planetary nebula) stars which are collectively known as UV-bright stars in galactic globular clusters. There are a number of differences between BHB and post-HB stars:

- The atmospheres of BHB stars are dominated by the affects of atomic diffusion (Michaud et al. 1983) and polluted by the products of partial CNO burning while post-HB stars can have much more complicated abundance patterns involving more advanced nuclear process and dust formation since they are more evolved.
- BHB stars have low rotational velocities so that their  $v\sin(i)$  values should be less than  $40 \text{ km s}^{-1}$  (Peterson 1983) while there are no established observational constraints on the  $v\sin(i)$  values of post-HB stars.
- BHB stars should have effective temperatures and gravities which place them on or near the horizontal branch on a theoretical HR-diagram. Post-HB stars can follow a number of tracks encompassing a wider range of gravities and effective temperatures (Figure 8).
- BHB stars are sub-luminous with respect to main-sequence stars so they will have received low kinematic scores in Table 6. This is not necessarily so for post-HB stars.

Given these differences we conclude that five of the old evolved stars are BHB stars, three are post-HB stars, and six are of “ambiguous” classification (Table 7). Any uncertainty in the classification a star as OES in Table 6 is propagated forward as an “?” appended to this classification. BD +13 3224 is a special case which is neither BHB or post-HB. Saio

& Jeffery (2000) conclude that this helium-rich pulsator is the product of a merger of two helium white dwarfs. We defer to their more exhaustive analysis.

The case of BD +33 2642 is explored in detail in Appendix A of Paper I. This star is known as a halo PPN (Napiwotzki 1993; Napiwotzki, Heber, & Koeppen 1994) with both classic nebular emission lines and a stellar photospheric absorption spectrum. It is iron deficient with enhancements of carbon, nitrogen, oxygen, and  $\alpha$ -process elements (Napiwotzki, Heber, & Koeppen 1994; Napiwotzki, Herrmann, Heber, & Altmann 2001; Martin 2004). The carbon and silicon abundances are very sensitive to the surface gravity and effective temperature used in the analysis (Martin 2004). Abundances of those elements are critical to deciphering the role of mixing, nuclear processing, and refractory grain formation in the stellar atmosphere. Even though BD +33 2642 is clearly a post-HB star with the beginnings of a planetary nebula, these uncertainties leave many open questions regarding its exact evolutionary status.

There is also notable uncertainty in the evolutionary status and classification of the stars with  $v\sin(i)$  greater than  $50 \text{ km s}^{-1}$ . These stars may be post-HB but they are classified as “ambiguous”. In these cases, rotational broadening hampers the abundance analysis because only the strongest lines can be measured and those may be blended. HD 40267, HD 105183, and BD +36 2268 all have reasonably well determined CNO abundances which show their photospheres have been significantly contaminated by fusion products. It is possible that these stars are normal Population I objects which were severely polluted by a nearby supernova *a la* BSS. However, BD +36 2268 and HD 105183 also have depressed silicon abundances which are well outside the range observed in normal Population I B stars. The photospheric abundances for HD 1112 are a confusing jumble so the most definitive thing we can conclude is that it is abnormal.

HD 233622 and HD 237844 are the most rapid rotators in the OES sample. They have silicon abundances, which like other OES stars, are depressed well below the normal range for B stars. Additionally HD 233622 has a kinematic score of 1 and its oxygen abundance (from two reliable lines) is raised slightly relative to the B star control sample. Unfortunately, we were not able to measure any CNO abundances for HD 237844 but it has an Si/S ratio which is exceptional. The abundances of both stars and the kinematic score of HD 233622 indicate that they are OES. However, their high  $v\sin(i)$ ’s imply that they cannot be low mass stars.



Table 7 includes the critical rotational velocities<sup>4</sup> calculated for the OES stars using the mass and radius from the tracks of Dorman et al. (1993) (see Table 9). Both HD 233622 and HD 237844 have  $v\sin(i)$ 's that are comparable to their critical rotation velocity. It is unlikely that a star so close to its critical velocity could exist in any stable configuration. However, if they are higher mass Population I stars (of 6 or 7  $M_{\odot}$ , see Table 2), then their critical velocities would be much higher and there would be no conflict.

HD 237844 has a space velocity consistent with ejection from the disk. However, HD 233622 has velocities which are much more extreme. Both have low silicon abundances which indicate that they could be low metallicity stars formed in situ in the halo. But their other abundances show additional anomalies and more evidence is needed to support such an extraordinary claim.

### 5.3. The Stars We Cannot Classify

Two of the stars in our sample (HD 121968 and HD 125924) have received a classification of “unknown” (U) due to insufficient information. Both have kinematics that are not consistent with Population I runaways (kinematic scores of 2; see Table 6) and no spectra or abundances. It is conceivable that they could be metal poor Population I stars formed in situ in the halo or BHB stars which have had their kinematics exaggerated (see Section 3.3). However, since there is no significant discrepancy between the flight times and main sequence lifetimes of these stars it is far more likely that the conclusions of Conlon et al. (1990) and Conlon et al. (1992) are correct and these are runaways ejected with enough force to accelerate their  $V_{\theta}$  and  $V_{\pi}$  far from the LSR.

### 5.4. Overlap With Other Studies

A number of the stars in our sample have been categorized individually or in small groups by other studies. In most cases those classifications agree with the classifications made here. The are: BD -15 115 (Ramspeck et al. 2001b; Magee et al. 2001; Conlon et al. 1992), Feige 40 (Conlon 1989a), HD 100340 (Ryans et al. 1999; Keenan et al. 1987; Conlon 1989a), HD 105183 (Dufton et al. 1993), PB 166 (de Boer et al. 1988; Conlon 1989a), Feige 84 (Lynn et al. 2004; Saffer et al. 1997), HD 123884 (Bidelman 1988), HD 137569

---

<sup>4</sup>The rotational velocity at which the centripetal acceleration at the equator is equal to the surface gravity of the star.  $v_{crit} = \sqrt{\frac{GM}{R}}$

(Danziger & Jura 1970), HD 138503 (Martin 2003), BD +33 2642 (See Paper I, Appendix A), HD 146813 (Conlon 1989a; Conlon et al. 1988), HD 149363 (Mdzinarishvili & Chargeishvili 2005), BD +13 3224 (Jeffery et al. 2001; Jeffery & Hill 1986), HD 206144 (Keenan et al. 1982), HD 218970 (Conlon 1989a; Conlon et al. 1989b), and HD 220787 (Keenan et al. 1982).

Our classification disagrees with those given for BD +36 2268 by Conlon et al. (1989b) and HD 149363 by Zboril & North (2000). We disagree with Zboril & North (2000) over the proper stellar atmospheric parameters for HD 149363 (for details see Paper I). For BD +36 2268, we agree with Conlon et al. (1989b) on the parameters we use in the abundance analysis and that there is no conflict between its flight time and main sequence lifetime. We also agree that the C abundance is depressed while N & O are “normal.” Taken with our Al, Si, and S data, this indicates to us that BD +36 2268 is a hot post-HB star rather than a Population I B star as asserted by Conlon et al.

Several other studies overlap with a substantial fraction of our sample. Ten of our stars were identified by Keenan & Dufton (1983) as Population I runaways based on their flight times. We agree that there are no significant conflicts between the flight times and main sequence lifetimes for any of those stars. However, we have classified two of them (HD 105183 and BD +36 2268) as old evolved stars based on their abundances.

Sixteen stars in our sample were also cited by Conlon et al. (1990) as stars with space velocities that imply they were ejected from the galactic disk. We agree that thirteen of these are Population I runaways and we have classified one other which could be a runaway as “unknown” (see Section 5.3). The remaining two are classified here as post-HB stars. While they have flight times that are consistent with their main sequence lifetimes, they also have peculiar abundance patterns (HD 105183 and BD +36 2268).

Allen & Kinman (2004) also assess the kinematics of sixteen stars in our sample. We only disagree with their assessment of HD 206144 which according to them has a flight time that significantly exceeds its main sequence lifetime. Our analysis shows that there is no inconsistency between the values we calculated for that star. It is unclear how Allen & Kinman (2004) computed their flight times or what model for the galactic potential they used so we do not know how our analysis differed from theirs.

Behr (2003) classified seventeen stars in this study according to their  $[\text{Fe}/\text{H}]$  and position relative to evolutionary tracks on a  $T_{eff}$  versus  $\log(g)$  diagram. The effective temperatures and surface gravities derived by Behr closely match the values that we have adopted (Paper I). There are no conflicts between our classifications and Behr’s for ten of the common stars.

We have classified HD 1112, HD 233622, HD 105183, and BD +36 2268 as “ambiguous”

old evolved stars while Behr classified them as “main sequence.” It is difficult to tell the difference between a main sequence and post-HB star on a  $T_{eff}$  versus  $\log(g)$  diagram. Our classification is primarily based on the abundance ratios of elements which Behr (2003) did not measure. In addition to that, each of these stars either have only marginal agreement between their flight times and main sequence lifetimes (BD +36 2268) or large  $V_\pi$  and/or  $V_\theta$  velocities assuming main sequence distances (HD 233622, HD 1112, and HD 105183) which imply that they are not runaway Population I stars.

Behr (2003) classified BD -7 230, BD +30 2355 and HD 213781 as “possible HB” because their  $T_{eff}$  and  $\log(g)$  are consistent with the horizontal branch and they have small  $v\sin(i)$ . We have classified each of these stars as Population I runaways based on their abundances. BD -7 230 is slightly metal poor ( $[Fe/H] \sim -0.4$ ), but this is not outside the range of values observed in the control sample of nearby Population I B stars. It also has a normal Mg/Fe ratio while every other BHB star in this sample is abnormal in that respect. In Paper I we discussed how a difference in the microturbulent velocity may have led Behr (2003) to significantly underestimate  $[Fe/H]$  for BD +30 2355 but otherwise we are in agreement with all the parameters that Behr derives for these stars. The abundances of these stars are not inconsistent with their classification as runaways and their kinematics assuming main sequence distances are very consistent with that population (each received a kinematic score of 4, see Section 5). Whereas if these were BHB stars there would be noticeable inconsistencies in their space velocities from overestimating their distances (see Section 3.3).

## 6. The Breakdown of High Latitude B Stars

Our sample is roughly magnitude limited by virtue of having been selected from the Hipparcos catalog (which is complete up to  $V \sim 10$ ) and the color-magnitude limited sample of Greenstein & Sargent (1974) (see Section 2, Paper I). As such, the overlap between this study and Greenstein & Sargent (1974) (32 stars with an FB number in Table 1 of Paper I) represent a sample that can be used to make rough conclusions about the proportion of Population I runaways and older evolved stars among the faint B stars at high galactic latitudes.

Table 8 compares our sample with the results from other similar surveys which like ours are roughly limited to stars with  $V$  magnitudes between 9 and 12. All these studies use abundance analysis and kinematics to classify the stars in their samples. Rolleston et al. (1997) use radial velocities alone while Magee et al. (2001), Ramspeck et al. (2001a), Ramspeck et al. (2001b), and our own study examined the full space velocities. Note that Rolleston et al. (1997) and Magee et al. (2001) are part of a comprehensive survey, while

Ramspeck et al. (2001a) and Ramspeck et al. (2001b) are randomly selected samples.

The only overlap between these studies and our own is runaway star BD -15 115 in Ramspeck et al. (2001b) and Magee et al. (2001). All of us find comparable proportions of runaway Population I stars and old evolved stars with no evidence of Population I stars formed in situ in the halo. There is remarkable agreement between our study and Magee et al. (2001) and Rolleston et al. (1997). The general consensus appears to be that about two thirds of all high galactic latitude B stars are high mass Population I runaways, while the remaining third are low mass older evolved stars.

## 7. Properties of the Population I Runaways

### 7.1. Runaway Binaries

The fraction of runaways with binary companions depends on the ejection mechanism which accelerated them. Simulations predict that 10% of stars ejected by DES are binary (Leonard & Duncan 1990). The runaway binaries produced by DES are pairs of normal main sequence stars observed as double lined spectroscopic binaries (SB2s). Whereas, binaries with captured neutron star companions should account for 20%–40% of runaways ejected by BSS (Portegies Zwart 2000). Therefore, a significant number of BSS runaways should be single-lined spectroscopic binaries (SB1s) with periods on the order of a few hundred days (Portegies Zwart 2000).

Almost all of the stars in this sample were observed at least twice over the course of a few days so the radial velocity measurements are sensitive to variations in short period binaries. The level of sensitivity is comparable to the errors given for the radial velocity in Table 2. They ranged from  $2 \text{ km s}^{-1}$  –  $15 \text{ km s}^{-1}$  depending on the number of lines measured and the  $v \sin(i)$  of the star. We detected the eclipsing binary HD 138503 (Martin 2003) but found no other short period binaries in our sample. HD 138503 was probably produced by DES since it is an SB2 composed of two main sequence stars.

In the case of five old evolved stars (HD 21305, HD 40267, HIP 41979, HD 237844, and HD 137569) and seven runaways (HD 21532, BD +61 996, HD 103376, BD +30 2355, HD 146813, HD 149363, and HD 206144) the observations were spread over several months so that they are sensitive to variations from longer period variables. We detected none except the known binary old evolved star HD 137569.

Finally, we compared the measured radial velocities with the literature (Table 4). Five runaways have radial velocities which differ from their literature values by more than two

sigma: HD 15910, Feige 40, HD 110166, HD 188618, and HD 216135. The radial velocities for HD 15190, Feige 40, and HD 110166 have very large errors so any discrepancy has a lower significance. HD 188618 and HD 216135 disagree rather significantly with previously published values. They are the best candidate SB1s in our sample. We are unable to verify that any of these are binaries.

The binary frequency observed by Gies & Bolton (1986) predicts about three binaries in a sample of 28 runaways. We found HD 138503 plus two promising candidates. Furthermore, those two promising candidates are most likely long period SB1s of the type expected for stars ejected by BSS (Portegies Zwart 2000). However, neither show any evidence that their photosphere was polluted by supernova ejecta (see Paper I).

Our results, taken by themselves, are not significant. However, a number of more extensive surveys have determined that fewer than 10% of early type high latitude runaways have binary companions (Gies & Bolton 1986; Philp et al. 1996; Sayer et al. 1996). That binary frequency is more consistent with simulations of DES than BSS.

## 7.2. Rotation of Runaway Stars & the Ejection Mechanisms

The rotational velocity distribution for high latitude B stars is roughly the same as nearby B stars in the field (Figure 10) with a slightly larger proportion of slow rotating stars since these samples include BHB stars (Magee et al. 1998). Other studies have biased their selection of runaway stars by using stellar rotation as a criterion to distinguish between BHB stars and “normal” Population I stars (i.e. Greenstein & Sargent (1974) and Behr (2003)). But we have not. There is no obvious correlation between the stars with small  $v_{\sin(i)}$  and the main sequence or horizontal branch (Figure 9). There are four slow  $v_{\sin(i)}$  stars clustered alone in the upper left corner of that diagram. However, three of those (HD 123844, HD 137569, and HIP 1511) are clearly OES based on their abundances and space velocities. Because the runaway star sample is selected without regard for projected rotational velocity ( $v_{\sin(i)}$ ) we are able to measure the unbiased rotational velocity distribution of runaway B stars.

Surprisingly, when the older evolved stars are removed from the distribution (Figure 10, panel B) there is a clear deficit of slow rotating stars compared to the field. It is highly unlikely that the field star samples of Wolff et al. (1982) and Guthrie (1984) are contaminated by slow rotating old evolved stars because both are drawn from main sequence B stars in the Yale Bright Star Catalog (Hoffleit & Jaschek 1982). Furthermore, Guthrie (1984) found that the field stars have the same distribution as “older” OB associations, which are not old

enough to contain any post-main sequence BHB or post-HB stars.

Our runaway star distribution appears to be more like the “youngest” Population I B stars from Guthrie (1984) (Figure 11). A Kolmogorov-Smirnov test (Kennedy & Neville 1986) shows that there is a 50% probability that our runaway sample was drawn from Guthrie’s “young” sub-group versus a 30% chance that it was drawn from Guthrie’s field star sample<sup>5</sup>. Guthrie’s “young” OB associations were selected for their high stellar density and Strom et al. (2005) and Huang & Gies (2005) have shown that denser star forming regions contain significantly fewer slow rotating stars. When one considers that dynamical ejection (DES) is more efficient in denser stellar environments, the implication is that most of the stars in our sample could have come from these tightly packed OB associations.

The BSS mechanism involves the ejection of a secondary from a close binary when the primary goes supernova. In the case of a close binary system there will be tidal locking, so that the rotation rate of the runaway will be directly related to its original orbital velocity. It is possible that the combination of the bias in our sample (which sharply excludes the smallest ejection velocities, see Section 2.2.2) and pre-ejection BSS tidal locking could produce a sample like ours with few slow rotators. However if BSS is the dominate mechanism at work in our sample, there should be a linear relationship between ejection velocity and  $v_{\text{sin}(i)}$  because the ejection velocity should be comparable to the orbital velocity when the system becomes unbound. There is clearly no trace of any relationship between rotation and ejection velocity in our sample (Figure 12). Therefore, it seems unlikely that BSS is the dominate mechanism which produced these runaways.

On the other hand, DES is much more efficient in densely populated environments (like Guthrie’s “young” OB associations) since it accelerates runaway stars through random dynamic interactions between stars or pairs of stars. Because the distribution of  $v_{\text{sin}(i)}$  for our sample so closely matches Guthrie’s “young” sub-groups it seems likely that DES is the dominate mechanism in our runaway sample.

Hoogerwerf et al. (2001) appears to contradict this notion by concluding that about two-thirds of massive runaways are produced by BSS. However, they surveyed a subset of stars within 700 pc of the Sun with space velocities up to  $115 \text{ km s}^{-1}$  that are mostly excluded from our sample. It is possible that these are a sub-population with different properties from the high latitude runaway B stars. Their classification scheme also assumed that BSS would produce runaways with larger rotational velocities and with flight times shorter than

---

<sup>5</sup>Adding one star to our runaways with a  $v_{\text{sin}(i)} \geq 180 \text{ km s}^{-1}$  increases the significance of the match with Guthrie’s “young” sub-group to over 80% with no change to the much lower probability of association with Guthrie’s field sample.

the estimated age of their “parent groups.” The former assumption was made without the benefit of the work of Strom et al. (2005) or the findings that we have reported here. The later neglects that DES can still occur in dense clusters as they age and expand, albeit at a lower rate.

### 7.3. The Missing Runaway Be Stars

If we assume that the frequency of Be stars is the same as reported by Zorec & Briot (1997) for the nearby field, this sample should have at least ten Be stars out of the 48 high latitude B stars in our sample. However, there are no classical Be stars in our sample<sup>6</sup>. This result is rather significant even considering that the number of Be stars will always be under-counted by a survey of this type. (Be emission is a transient phenomenon that can be missed by surveys with short temporal baselines.)

Two surveys have identified runaway Be stars at smaller distances from the galactic plane. Slettebak et al. (1997) identified 8 runaway Be stars between 0.2–0.9 kpc from the plane which barely overlaps the volume occupied by most of our sample and contains mostly runaways that would have been ejected with  $V_{ej}$  too low to be included in our sample. Likewise, Berger & Gies (2001) found 3%–7% of the Be stars in the Hipparcos catalog have runaway space velocities. However those velocities ranged from 40 km s<sup>-1</sup> – 102 km s<sup>-1</sup> which would have only a small overlap with our sample. Both these studies imply that the incidence of Be stars among runaways is lower than measured in the field.

A population of B stars which do not exhibit the Be phenomenon could prove invaluable for identifying the critical factors involved. Obviously, fast rotation alone does not create Be stars since on average most runaways rotate faster than B stars found in the field (see Section 7.2). Berger & Gies (2001) conjectured that mass transfer during the post main sequence phase of a binary system prior to BSS might play a role in the Be phenomenon. There is a low incidence among runaways of binaries that could transfer mass at critical times (see Section 7.1). However, it appears that most of these stars were ejected by DES. By process of elimination, it remains that this could somehow be tied to the small number of binaries or the origin of the runaways in dense star clusters with some mechanism selecting against the Be phenomenon there.

McSwain & Gies (2005) found no correlation between the number of Be stars and stellar

---

<sup>6</sup>The spectrum of Feige 23 has narrow NaD emission lines (see Paper I, Fig. 12) but no Hydrogen Balmer emission.

density in galactic star clusters. But they did find a smaller frequency of Be stars (2%–7%) in clusters than reported in the field by Abt (1987) and Zorec & Briot (1997). They give three reasons for this discrepancy:

1. Magnitude limited field samples are biased in favor of early type B stars in Gould’s Belt and early spectral types have a higher Be frequency.
2. Gould’s Belt is also a population that has a higher frequency of Be stars due to its age.
3. McSwain & Gies made one-shot observations of their clusters which tend to underestimate the actual number of Be stars.

However, the fact remains that Berger & Gies (2001) also found a lower incidence of Be stars among runaways than in the field. Also like McSwain & Gies (2005), we do not have a long baseline of data which will catch temporarily inactive Be stars. If, as implied by the  $v\sin(i)$  distribution, the runaways are ejected mainly from cluster environments and we assume Be stars are produced in the smaller proportions measured by McSwain & Gies (2005) or Berger & Gies (2001), then it is much more likely that our sample of 49 stars with 31 Population I runaways would not contain any Be stars.

## 8. Properties of the Old Evolved Stars

### 8.1. Revised Kinematics of BHB Stars

The distances and space velocities of the low mass evolved stars in the sample were initially exaggerated by estimating their photometric parallax from a main sequence luminosity (see Section 3.3). Now that the BHB stars are identified, their photometric parallax and space velocities can be recalculated using more appropriate absolute magnitudes from the evolutionary tracks of Dorman et al. (1993) for the appropriate effective temperatures, surface gravities, and metallicities (Table 9) and the bolometric corrections calculated by ATLAS12. HD 21305 has a very small proper motion so a factor of five change in its distance has very little effect on its space velocity. However, the space velocities of HIP 1511, HIP 41979, PB 166, and HD 222040 are markedly different. The revised space velocities for these stars are much more reasonable than those listed in Table 5.

It is easy to chemically and kinematically assign HIP 1511 and HD 222040 membership in the halo population and likewise assign HD 21305 membership in the thick disk population. HIP 41979 and PB 166 have abundances which are consistent with the thick disk but their revised  $V_\pi$  and  $V_z$  do not comfortably fit in the expected velocity distribution for the thick



disk population (Table 1). The uncertainty of the distances and the proper motions have significant influence over  $V_\pi$  and  $V_z$  for both stars. Based only on  $V_\theta$  it seems likely that both are members of the thick disk population.

We also recalculated the distances and space velocities of the post-HB and “ambiguous” evolved stars using the Dorman et al. tracks (Table 9). Because there is a chance that the stars labeled “ambiguous” could be main sequence stars, we have included their main sequence distances and velocities for comparison. In the case of non-BHB stars we are less certain that the tracks give the true luminosities because we are unsure if they match that evolutionary state. The Dorman et al. tracks yield distances of 2.4 kpc and 0.83 kpc for BD +33 2642 and BD +13 3224 respectively. However, those values are significantly different from the distances obtained independently by Napiwotzki, Heber, & Koeppen (1994) (3.30 kpc) and Jeffery et al. (2001) (1.70 kpc). We have used those more reliably determined distances from the literature to calculate the space velocities for those stars. In any case, when we use these distances to calculate the space velocities of the post-HB and “ambiguous” stars all of them appear to be members of the galactic thick disk population except BD +33 2642, which is probably a member of the halo population.

## 8.2. Metal-Rich BHB Stars

In Paper I, we identified three metal-rich BHB stars from their abundance patterns which are heavily influenced by atomic diffusion: HD 21305, HIP 41979, and PB 166. The analysis of the space velocities of HIP 41979 and PB 166 confirm they are BHB stars. In the case of HD 21305, its effective temperature and gravity are not consistent with a horizontal branch star. The space velocity of HD 21305 indicates that it is probably a member of the galactic thick disk population regardless of its evolutionary state (see Section 8.1). Therefore, its BHB classification is made entirely based on its abundance pattern and hence, is less certain than the other two metal-rich BHB stars.

## 9. Conclusions

We have sorted the high galactic latitude stars in our sample into five groups: Population I runaways (31 stars), BHB stars (5 stars), post-HB stars (3 stars), old evolved stars of ambiguous classification (6 stars), and those that we cannot classify (2 stars). The two unclassified stars are probably extreme Population I runaways.

We agree with other studies that roughly two thirds of faint high galactic latitude B

stars are Population I runaways ejected from the galactic disk. The remainder are older evolved post-main sequence stars. No star in this sample (or any other we are aware of) shows metal poor abundances and halo-like kinematics of a young massive star which formed in situ in the galactic halo. HD 237840 and HD 233622 are classified as old evolved stars based on their abundances. However they are rotating far too rapidly to be low mass stars. They could be chemically odd Population I runaways or main sequence stars formed in situ in the halo but there is not enough evidence to justify either alternative.

The Population I runaways have a number of interesting properties:

- A low incidence of binaries (less than 10% as shown in other studies).
- A deficit of slow rotators ( $v\sin(i) < 50 \text{ km s}^{-1}$ ) compared to the field.
- No Be stars.

No significant shift was measured in the radial velocities of the 31 runaways in the sample over baselines of a few days or months except for HD 137569 and the eclipsing binary HD 138503 (IT Lib). That binary was probably launched by DES since it is an SB2 comprised of two normal main sequence stars. Two stars (HD 188618 and HD 216135) have discrepancies between their measured radial velocities and those reported in the literature. These could be single-lined spectroscopic binaries (SB1s) with neutron star companions produced by BSS with periods on the order of several hundred days. These results are not significant by themselves but they are consistent with more extensive studies which show that the binary frequency among early type runaways is less than 10%. This relative lack of runaway binaries implies that DES is the dominant mechanism. The projected rotational velocity ( $v\sin(i)$ ) distribution also supports this hypothesis.

The rotation of Population I runaways are like densely populated star clusters in that they have fewer slow rotators than the field population. Therefore, we conclude that most of the runaways originate in dense clusters or star forming regions. This supports the DES hypothesis since it is much more efficient in dense stellar environments. There is also no correlation between ejection velocity ( $V_{ej}$ ) and  $v\sin(i)$ , as would be expected for a BSS dominated sample.

Together, the low frequency of binaries and the lack of slow rotators provide a compelling argument that DES is the dominant ejection mechanism for runaway B stars. This is not to say that BSS does not contribute at some level. HD 188618 and HD 215135 could be long period SB1s of the type produced by BSS. However, it appears that runaways accelerated by DES dominate this sample.

The absence of Be stars from the sample presents another interesting facet. This could be due to an observational bias either on our part or affecting field star samples. But it could also potentially be due to some mechanism responsible for the Be phenomenon that runaways do not possess. The lack of binary companions, something about the ejection mechanism, or another factor in the cluster environment which they were ejected from may leave runaways without crucial ingredients necessary to become Be stars. Further study of runaways could help unlock the mystery of the Be phenomenon.

The old evolved stars also exhibit interesting characteristics. The velocities of the BHB stars determine their membership in either the thick disk or halo populations. We confirmed that PB 166 and HIP 41979 are nearby solar-metallicity BHB stars which belong to the thick disk. There is still some uncertainty about HD 21305 which has a pattern of abundances like the other two and kinematically belongs to the thick disk. However its  $\log(g)$  and  $T_{eff}$  place it well away from the TAHB.

## 10. Acknowledgments

I wish to extend hearty thanks to R.E. Luck for his support of this work as my PhD adviser and his input on this publication. Thank you also to the other members of my PhD committee for their critical comments on my dissertation: H. Morrison, J.C. Mihos, and R. Dunbar. I also thank P. Harding for generously sharing his galactic potential integrator and V. McSwain and S. Wolff for their very useful comments and discussion concerning Be star populations, star clusters, and stellar rotation. Thank you also to the anonymous referee whose critical comments helped polish this publication. I feel this work was strengthened by their diligence and willingness to give significant time and effort without credit to their name. Last but not least, I want to thank Kris Davidson and Roberta Humphreys for providing me with the time, environment, and encouragement to finish distilling this research into a publishable form. This work was supported in part by the Jason J. Nassau Scholarship Fund and the Townsend Fund through the generous continued support of the Ford, Nassau, and Townsend families.

## REFERENCES

- Abt, H. A. 1987, IAU Colloq. 92: Physics of Be Stars, 470
- Allen, C., & Kinman, T. 2004, Revista Mexicana de Astronomia y Astrofisica Conference Series, 21, 121
- Barbier-Brossat, M., & Figon, P. 2000, A&AS, 142, 217
- Behr, B. B. 2003, ApJS, 149, 101
- Berger, D. H., & Gies, D. R. 2001, ApJ, 555, 364
- Bidelman, W. P. 1988, PASP, 100, 1084
- Binney, J., & Merrifield, M. 1998, Galactic astronomy / James Binney and Michael Merrifield. Princeton, NJ : Princeton University Press, 1998. (Princeton series in astrophysics) QB857 .B522 1998
- Blaauw, A. 1961, Bull. Astron. Inst. Netherlands, 15, 265
- Bolton, C. T. & Thomson, J. R. 1980, ApJ, 241, 1045
- Brown, P. J. F., Dufton, P. L., Keenan, F. P., Boksenberg, A., King, D. L., & Pettini, M. 1989, ApJ, 339, 397
- Carney, B. W., Laird, J. B., & Latham, D. W. 1988, AJ, 96, 560
- Conlon, E. S., Brown, P. J. F., Dufton, P. L., & Keenan, F. P. 1988, A&A, 200, 168
- Conlon, E. S. 1989a, Irish Astronomical Journal, 19, 59
- Conlon, E. S., Brown, P. J. F., Dufton, P. L., & Keenan, F. P. 1989b, A&A, 224, 65
- Conlon, E. S., Dufton, P. L., Keenan, F. P., & Leonard, P. J. T. 1990, A&A, 236, 357
- Conlon, E. S., Dufton, P. L., Keenan, F. P., McCausland, R. J. H., & Holmgren, D. 1992, ApJ, 400, 273
- Cramer, N. 1999, New Astronomy Review, 43, 343
- Cramer, N. & Maeder, A. 1979, A&A, 78, 305
- de Boer, K. S., Richtler, T., & Heber, U. 1988, A&A, 202, 113
- Danziger, I. J. & Jura, M. A. 1970, ApJ, 161, 997

- Drimmel, R. & Spergel, D. N. 2001, *ApJ*, 556, 181
- Dorman, B., Rood, R. T., & O’Connell, R. W. 1993, *ApJ*, 419, 596
- Dufton, P. L., Conlon, E. S., Keenan, F. P., McCausland, R. J. H., & Holmgren, D. E. 1993, *A&A*, 269, 201
- Duflot, M., Figon, P., & Meyssonier, N. 1998, *VizieR Online Data Catalog*, 3190, 0
- Edvardsson, B., Andersen, J., Gustafsson, B., Lambert, D. L., Nissen, P. E., & Tomkin, J. 1993, *A&A*, 275, 10
- Eggen, O. J. 1961, *Royal Greenwich Observatory Bulletin*, 41, 245
- Evans, D. S. 1967, *IAU Symp. 30: Determination of Radial Velocities and their Applications*, 30, 57
- Fabricius, C. 1993, *Bulletin d’Information du Centre de Donnees Stellaires*, 42, 5
- Fekel, F. C. 1999, *Astronomical Society of the Pacific Conference Series*, 185, 378
- Gies, D. R., & Bolton, C. T. 1986, *ApJS*, 61, 419
- Graham, J. A., & Slettebak, A. 1973, *AJ*, 78, 295
- Greenstein, J. L. & Sargent, A. I. 1974, *ApJS*, 28, 157
- Grenier, S., et al. 1999, *A&AS*, 137, 451
- Guthrie, B. N. G. 1984, *MNRAS*, 210, 159
- Harding, G. A., Fahim, F., & Haslam, C. M. 1971, *Royal Greenwich Observatory Bulletin*, 165, 257
- Harding, P., Morrison, H. L., Olszewski, E. W., Arabadjis, J., Mateo, M., Dohm-Palmer, R. C., Freeman, K. C., & Norris, J. E. 2001, *AJ*, 122, 1397
- Heger, A. & Langer, N. 2000, *ApJ*, 544, 1016
- Heger, A., Langer, N., & Woosley, S. E. 2000, *ApJ*, 528, 368
- Helmi, A. & White, S. D. M. 2001, *MNRAS*, 323, 529
- Hernquist, L. 1990, *ApJ*, 356, 359

- Hoffleit, D., & Jaschek, C. 1982, *The Bright Star Catalogue*, New Haven: Yale University Observatory (4th edition), 1982
- Høg, E. et al. 2000, *A&A*, 355, L27 (Tycho-2)
- Holmberg, J., & Flynn, C. 2004, *MNRAS*, 352, 440
- Hoogerwerf, R., de Bruijne, J. H. J., & de Zeeuw, P. T. 2001, *A&A*, 365, 49
- Huang, W., & Gies, D. R. 2005, *ArXiv Astrophysics e-prints*, arXiv:astro-ph/0510450
- Hurley, J. R., Pols, O. R., & Tout, C. A. 2000, *MNRAS*, 315, 543
- Iben, I. J. & Tutukov, A. V. 1997, *ApJ*, 491, 303
- Jeffery, C. S. & Hill, P. W. 1986, *MNRAS*, 221, 975
- Jeffery, C. S., Woolf, V. M., & Pollacco, D. L. 2001, *A&A*, 376, 497
- Johnston, K. V., Spergel, D. N., & Hernquist, L. 1995, *ApJ*, 451, 598
- Johnston, K. V., Spergel, D. N., & Haydn, C. 2002, *ApJ*, 570, 656
- Keenan, F. P., Dufton, P. L., & McKeith, C. D. 1982, *MNRAS*, 200, 673
- Keenan, F. P., & Dufton, P. L. 1983, *MNRAS*, 205, 435
- Keenan, F. P., Brown, P. J. F., Conlon, E. S., Dufton, P. L., & Lennon, D. J. 1987, *A&A*, 178, 194
- Kennedy, J. B. & Neville, A. M. 1986, *Basic Statistical Methods for Engineers and Scientists*, 3rd edition, (New York: Harper & Row)
- Kent, S. M., Dame, T. M., & Fazio, G. 1991, *ApJ*, 378, 131
- Kilkenny, D., & Hill, P. W. 1975, *MNRAS*, 172, 649
- Kuijken, K. & Gilmore, G. 1989, *MNRAS*, 239, 605
- Kuijken, K. & Gilmore, G. 1991, *ApJ*, 367, L9
- Kurucz, R. L. 1996, *ASP Conf. Ser. 108: M.A.S.S., Model Atmospheres and Spectrum Synthesis*, 108, 160
- Leonard, P. J. T. & Duncan, M. J. 1990, *AJ*, 99, 608

- Leonard, P. J. T. 1991, *AJ*, 101, 562
- Lynas-Gray, A. E., Schoenberner, D., Hill, P. W., & Heber, U. 1984, *MNRAS*, 209, 387
- Lynn, B. B., et al. 2004, *MNRAS*, 353, 633
- Magee, H. R. M., et al. 1998, *A&A*, 338, 85
- Magee, H. R. M., et al. 2001, *MNRAS*, 324, 747
- Martin, J. C. & Morrison, H. L. 1998, *AJ*, 116, 1724
- Martin, J. C. 2003, *PASP*, 115, 49
- Martin, J. C. 2004, *AJ*, 128, 2474 (Paper I)
- McSwain, M. V. & Gies, D. R. 2005, *ApJS*, in press
- Mdzinarishvili, T. G., & Chargeishvili, K. B. 2005, *A&A*, 431, L1
- Michaud, G., Vauclair, G., & Vauclair, S. 1983, *ApJ*, 267, 256
- Mihalas, D. & Binney, J. 1981, San Francisco, CA, W. H. Freeman and Co., 1981. 608
- Miyamoto, M. & Nagai, R. 1975, *PASJ*, 27, 533
- Napiwotzki, R., Herrmann, M., Heber, U., & Altmann, M. 2001, *Post-AGB Objects as a Phase of Stellar Evolution*, 277
- Napiwotzki, R., Heber, U., & Koepfen, J. 1994, *A&A*, 292, 239
- Napiwotzki, R. 1993, *Acta Astronomica*, 43, 415
- Perryman, M. A. C. & ESA 1997, *The Hipparcos and Tycho catalogues. Astrometric and photometric star catalogues derived from the ESA Hipparcos Space Astrometry Mission*, Publisher: Noordwijk, Netherlands: ESA Publications Division, 1997, Series: ESA SP Series vol no: 1200, ISBN: 9290923997 (HIP)
- Perrot, C. A., & Grenier, I. A. 2003, *A&A*, 404, 519
- Peterson, R. C. 1983, *ApJ*, 275, 737
- Philp, C. J., Evans, C. R., Leonard, P. J. T., & Frail, D. A. 1996, *AJ*, 111, 1220
- Poveda, A., Ruiz, J., & Allen, C. 1967, *Bol. Obs. Tonantzinta Tacubaya*, 4, 86

- Portegies Zwart, S. F. 2000, *ApJ*, 544, 437
- Ramspeck, M., Heber, U., & Edelmann, H. 2001a, *A&A*, 379, 235
- Ramspeck, M., Heber, U., & Moehler, S. 2001n, *A&A*, 378, 907
- Rolleston, W. R. J., et al. 1997, *MNRAS*, 290, 422
- Ryans, R. S. I., Keenan, F. P., Rolleston, W. R. J., Sembach, K. R., & Davies, R. D. 1999, *MNRAS*, 304, 947
- Saio, H., & Jeffery, C. S. 2000, *MNRAS*, 313, 671
- Saffer, R. A., Keenan, F. P., Hambly, N. C., Dufton, P. L., & Liebert, J. 1997, *ApJ*, 491, 172
- Sayer, R. W., Nice, D. J., & Kaspi, V. M. 1996, *ApJ*, 461, 357
- Schaller, G., Schaerer, D., Meynet, G., & Maeder, A. 1992, *A&AS*, 96, 269
- Schoenberner, D. 1979, *A&A*, 79, 108
- Slettebak, A., Wagner, R. M., & Bertram, R. 1997, *PASP*, 109, 1
- Spergel, D. N., Malhotra, S., & Blitz, L. 1996, *Spiral Galaxies in the Near-IR*, Proceedings of the ESO/MPA Workshop Held at Garching, Germany, 7-9 June 1995 edited by Dante Minniti and Hans-Walter ix. Springer-Verlag Berlin Heidelberg New York. Also ESO Astrophysics Symposia (European Southern Observatory), 1996., 128
- Strom, S. E., Wolff, S. C., & Dror, D. H. A. 2005, *AJ*, 129, 809
- Stothers, R., & Frogel, J. A. 1974, *AJ*, 79, 456
- Tout, C. A., Pols, O. R., Eggleton, P. P., & Han, Z. 1996, *MNRAS*, 281, 257
- Urban, S. E., Corbin, T. E., & Wycoff, G. L. 1997, *VizieR Online Data Catalog*, 1246 (ACT)
- Wolff, S. C., Edwards, S., & Preston, G. W. 1982, *ApJ*, 252, 322
- Zacharias, N. et al. 2000, *AJ*, 120, 2131 (UCAC)
- Zboril, M. & North, P. 2000, *Contributions of the Astronomical Observatory Skalnaté Pleso*, 30, 12
- Zorec, J., & Briot, D. 1997, *A&A*, 318, 443
- Zwicky, F. 1957, Berlin: Springer, 1957





## A. Computing Trajectories in the Galactic Potential

The orbital integrator we use is described in detail by Harding et al. (2001). The Milky Way’s potential was simulated following the prescription of Johnston et al. (1995) using a three component model which combines: (1) a Miyamoto & Nagai (1975) disk potential, (2) a Hernquist (1990) spheroidal potential, (3) and a logarithmic dark halo potential. The parameters for each of the components are selected so that together they reproduce the observed rotation curve of the Milky Way’s disk (Table 10). Harding et al. (2001), Johnston et al. (2002), Helmi & White (2001) have used the same model and parameters to successfully simulate the motions of stars in the galactic halo. This model and integrator also reasonably reproduce the results of Magee et al. (2001) from their data (Table 11) within the margin of error we would expect since they use a different galactic potential model.

The parameters of the galactic potential model affect the flight times of runaways from the galactic plane. The disk component of the model provides most of the restoring force that governs the ballistic trajectories calculated for each star. Therefore, it is a matter of concern that the mass surface density of the galactic disk we have adopted in our model for this study ( $\Sigma_{disk} = 95 \text{ M}_{\odot} \text{ pc}^{-2}$ ) is more than twice the local mass surface density of the disk alone ( $\Sigma_{disk} = 48 \pm 9 \text{ M}_{\odot} \text{ pc}^{-2}$ , Kuijken & Gilmore (1989);  $\Sigma_{disk} = 56 \pm 6 \text{ M}_{\odot} \text{ pc}^{-2}$ , Holmberg & Flynn (2004)) and about four thirds the total integrated mass density within 1.1 kpc of the galactic plane ( $\Sigma_{disk} = 71 \pm 6 \text{ M}_{\odot} \text{ pc}^{-2}$ , Kuijken & Gilmore (1991);  $\Sigma_{disk} = 74 \pm 6 \text{ M}_{\odot} \text{ pc}^{-2}$ , Holmberg & Flynn (2004)).

In simple terms, a decrease in  $\Sigma_{disk}$  should produce a proportional increase in the flight times of the stars in the sample. A smaller  $\Sigma_{disk}$  translates into a smaller restoring force for stars displaced from the galactic plane, allowing runaway stars with a given ejection velocity to travel further from the disk. This means that stars would travel at lower velocities to reach the same positions, lengthening their flight times. The disk potential is embedded in the larger halo potential, so stars that journey beyond the immediate influence of the disk would be less effected by changes in  $\Sigma_{disk}$ . For this reason, this effect should be greater for stars nearer to the disk moving with slower initial ejection velocities than for stars with higher initial ejection velocities further from the plane.

The adopted potential model (Table 10) relies on a balance between its three components in order to reproduce the observed rotation curve of the galactic disk. Therefore, a complete reformulation of the model is beyond the scope of this study. However, a simple reassessment gives an reliable estimate of the effect that a lower  $\Sigma_{disk}$  might have on the calculated flight times. In a simple-minded way, we lowered  $\Sigma_{disk}$  by altering the parameters for the disk component and then adjusted the bulge and halo components to flatten the galactic rotation curve as near to  $210 \text{ km s}^{-1}$  as possible between 5 kpc and and 20 kpc from the galactic

center. In three of the models  $\Sigma_{disk}$  was altered by changing the total mass of the disk ( $M_{disk}$ ). However a fourth model label "Short Disk" was produced by adopting a shorter disk scale length favored by Kent, Dame, & Fazio (1991), Spergel et al. (1996), Drimmel & Spergel (2001), and references therein. The parameters for each model are given in Table 12.

The flight times were recalculated for each star in the sample using the alternate models. Figure 13 shows the effect of each model on the calculated flight times versus distance of the star from the galactic plane. The No Bulge model is identical to the original model except that it has no bulge component. Panel A confirms that the bulge component has no significant effect on the calculated flight times. The results from the Short Disk model (panel E) are similar to the 0.50 Disk model (panel B) which has the same  $\Sigma_{disk}$ . This leads us to conclude that the flight times are not very sensitive to the disk scale length except through its influence on  $\Sigma_{disk}$ .

Panels B through D demonstrate that reducing  $\Sigma_{disk}$  lengthens the flight times for stars in the sample. The transition between stars dominated by the disk and the halo occurs at about 1.5 kpc from the galactic plane. The flight times for stars more than 1.5 kpc from the galactic plane are at most ten to fifteen percent larger while stars that are within 1.5 kpc of the disk have much larger differences in calculated flight times dependent on  $\Sigma_{disk}$ .

The differences in travel time between the original model and the 0.5 Disk model (B) affect the relationship between each star's flight time and main sequence lifetime (Figure 14). Fortunately, most stars remain within the same region defined by the dotted lines if  $\Sigma_{disk}$  is halved. Therefore, we conclude that changes to the parameters of the galactic potential within the range of values discussed by the literature have no affect on the classification of stars in our sample.

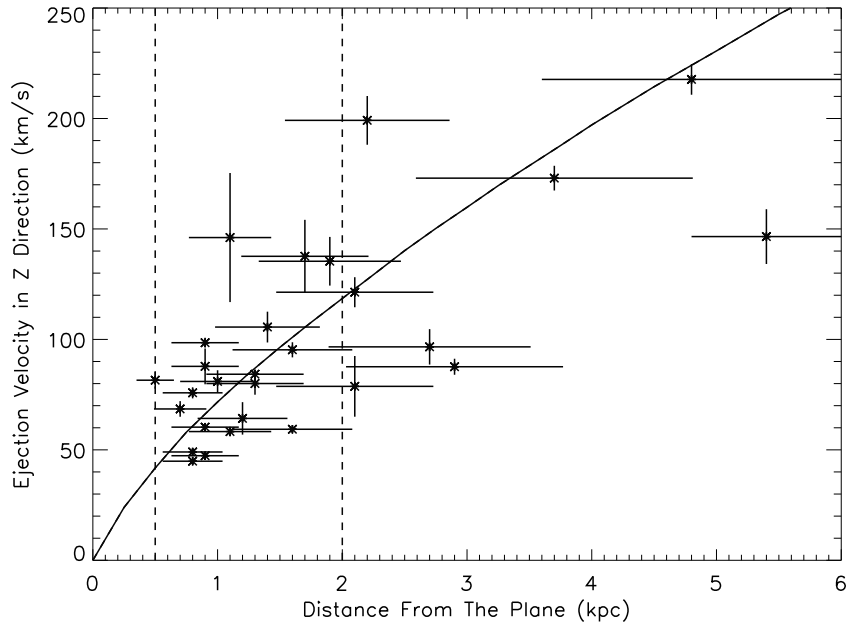


Fig. 1.— A plot of the Population I runaway stars in the sample. The solid curve is the theoretical maximum Z-distance which a star will reach with a given  $Z_{ej}$ . The dashed vertical lines mark  $0.5 \text{ kpc} \leq Z \leq 2.0 \text{ kpc}$ .

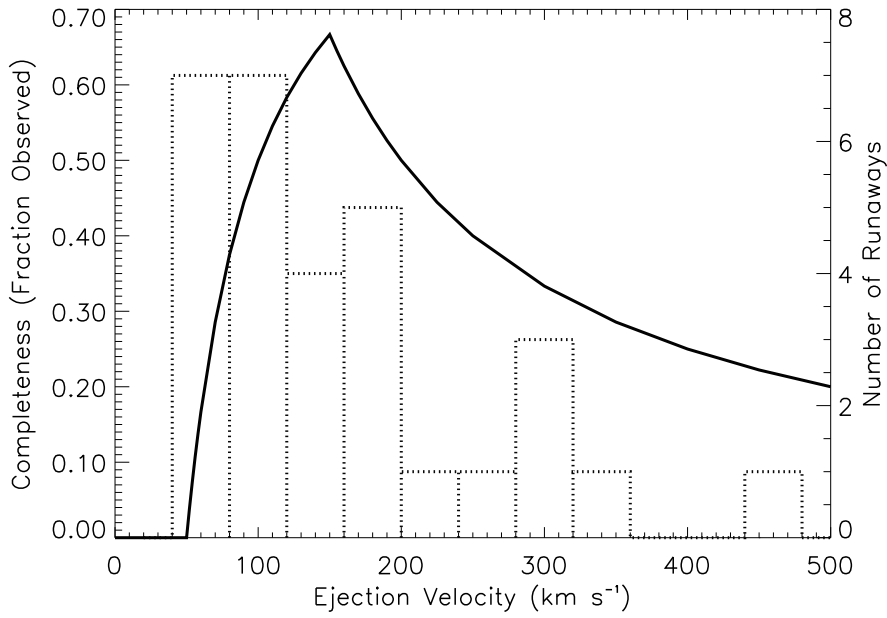


Fig. 2.— The results of a Monte Carlo simulation of the selection effect with regard to ejection velocity ( $V_{ej}$ ) in the sample (solid curve read off the left axis) and a histogram of the runaway ejection velocities in  $40 \text{ km s}^{-1}$  bins (dotted line read off the right axis).

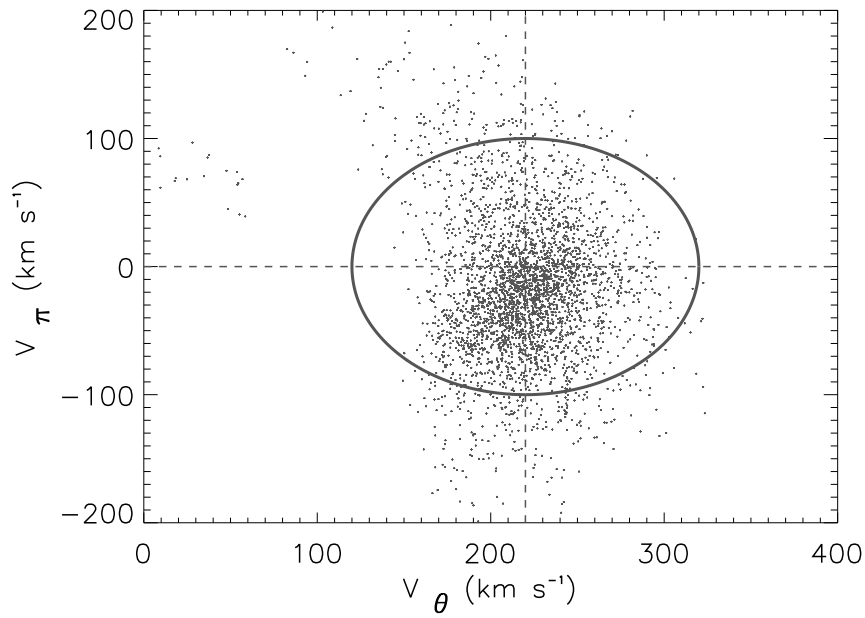


Fig. 3.— The results of a Monte Carlo simulation of the expected  $V_\pi$  versus  $V_\theta$  distribution for stars ejected from the solar neighborhood included in our sample. The dashed lines mark the LSR at  $(V_\theta, V_\pi) = (220 \text{ km s}^{-1}, 0 \text{ km s}^{-1})$ . The circle centered on the LSR has a radius of  $100 \text{ km s}^{-1}$ .

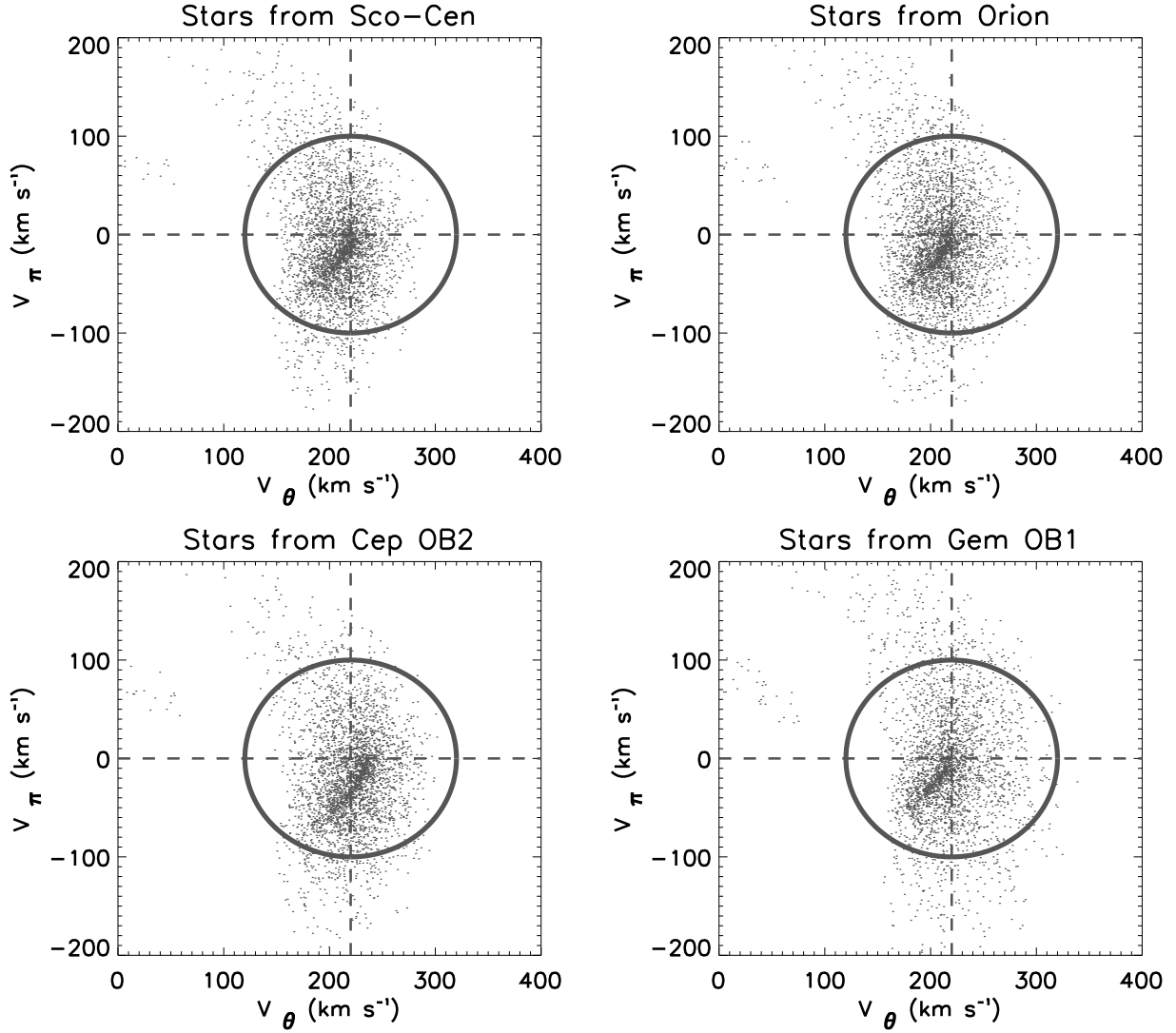


Fig. 4.— The results of a Monte Carlo simulation of the expected  $V_\pi$  versus  $V_\theta$  distribution for stars ejected from specific star forming regions in the solar neighborhood. The circle centered on the LSR has a radius of 100  $\text{km s}^{-1}$ .

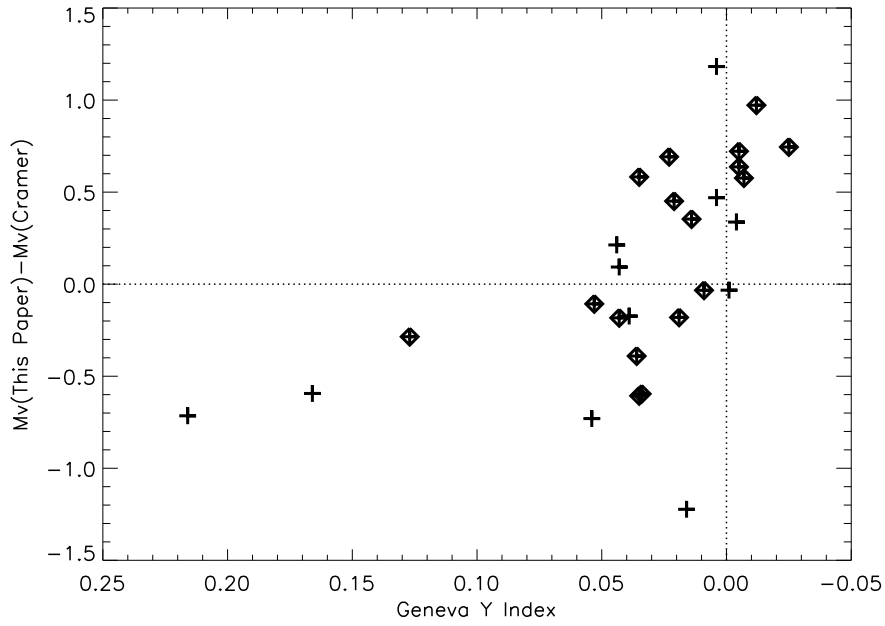


Fig. 5.— The difference between the absolute magnitudes derived by our method and Cramer (1999) versus the Geneva Y index for each star. Stars which are later classified as Population I runaways are highlighted with diamond shapes.



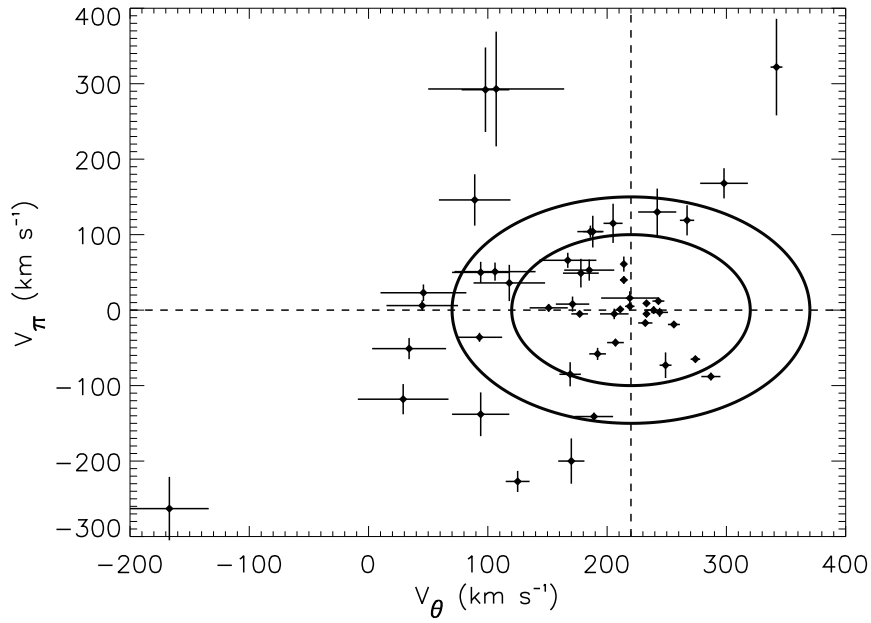


Fig. 6.— A plot of  $V_\pi$  versus  $V_\theta$  for stars in the sample assuming main sequence distances. The dashed lines mark the LSR at  $(V_\pi, V_\theta) = (0 \text{ km s}^{-1}, 220 \text{ km s}^{-1})$ . The circles centered on the LSR are drawn with radii of  $100 \text{ km s}^{-1}$  and  $150 \text{ km s}^{-1}$ .

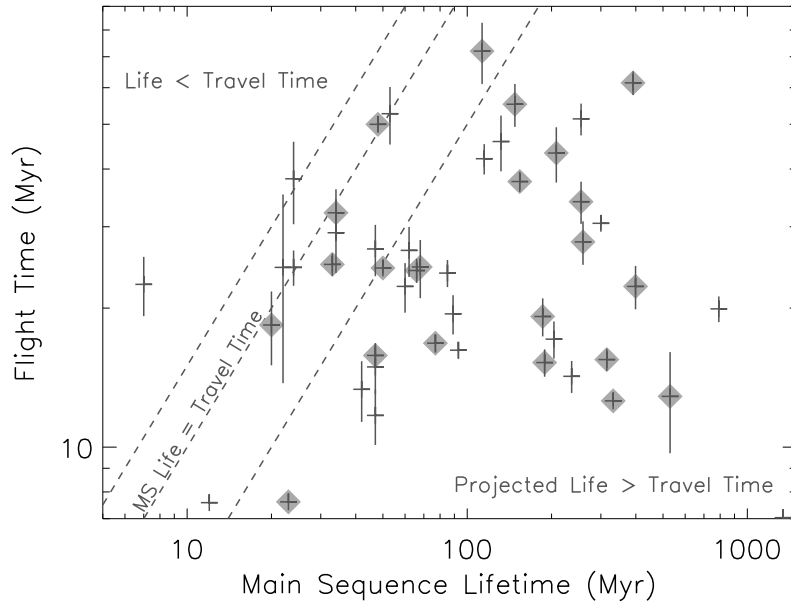


Fig. 7.— The flight time ( $T_{flight}$ ) from the disk (assuming main sequence distances) plotted against the estimate of the main sequence lifetime. Stars inside the circled region from Figure 6 are highlighted with a filled diamond.

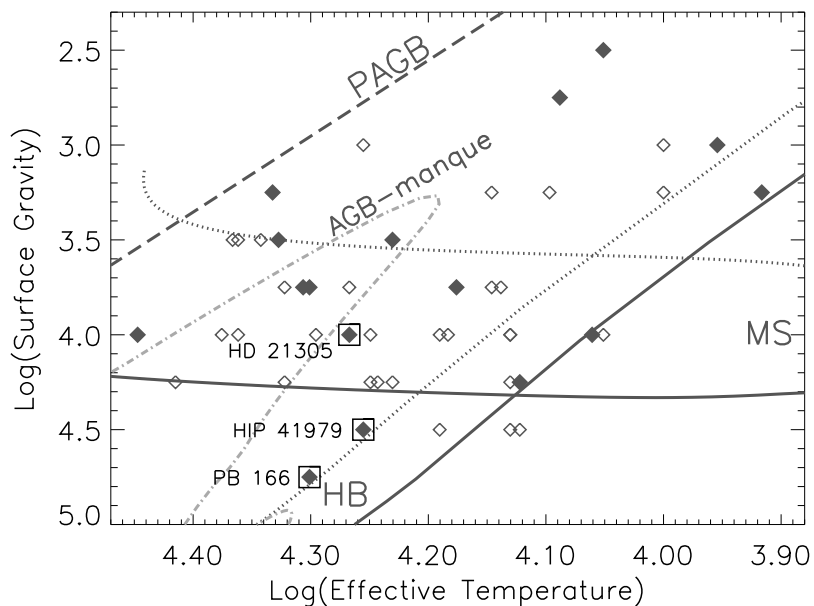


Fig. 8.— A plot of the effective temperatures and surface gravities of the post-main sequence program stars (filled diamonds) and runaway main sequence star (smaller open diamonds) compared to the position of the zero age (solid line) and terminal age (dotted line) Main Sequence (Tout et al. 1996; Hurley et al. 2000), the zero age (solid line) and terminal age (dotted line) Horizontal Branch (Dorman et al. 1993), a representative post-asymptotic branch track for a star of  $0.6 M_{\odot}$  after AGB mass-loss (dashed line) (Schoenberner 1979), and a representative AGB-manqué track from the Dorman et al. (1993) E64 model starting with a HB mass of  $0.505 M_{\odot}$  (light dash-dot line). The tracks are for solar metallicity ( $[Fe/H] = 0$ ) except the AGB-manqué track which is  $[Fe/H] = -1.48$ . The stars HD 21305, HIP 41979, and PB 166 are highlighted for Section 8.2.

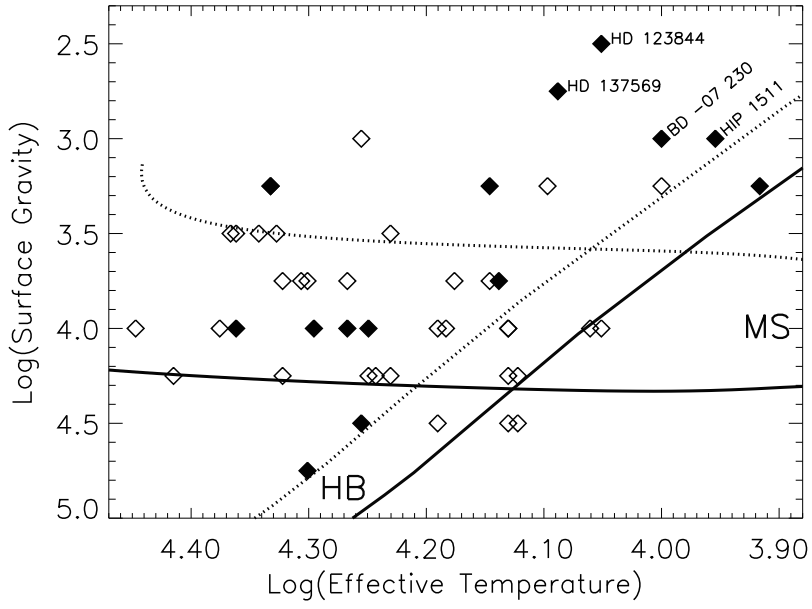


Fig. 9.— Similar to Figure 8. Solid diamonds: stars with  $v \sin(i) \leq 40 \text{ km s}^{-1}$ . Open diamonds: stars with  $v \sin(i) \geq 40 \text{ km s}^{-1}$ .

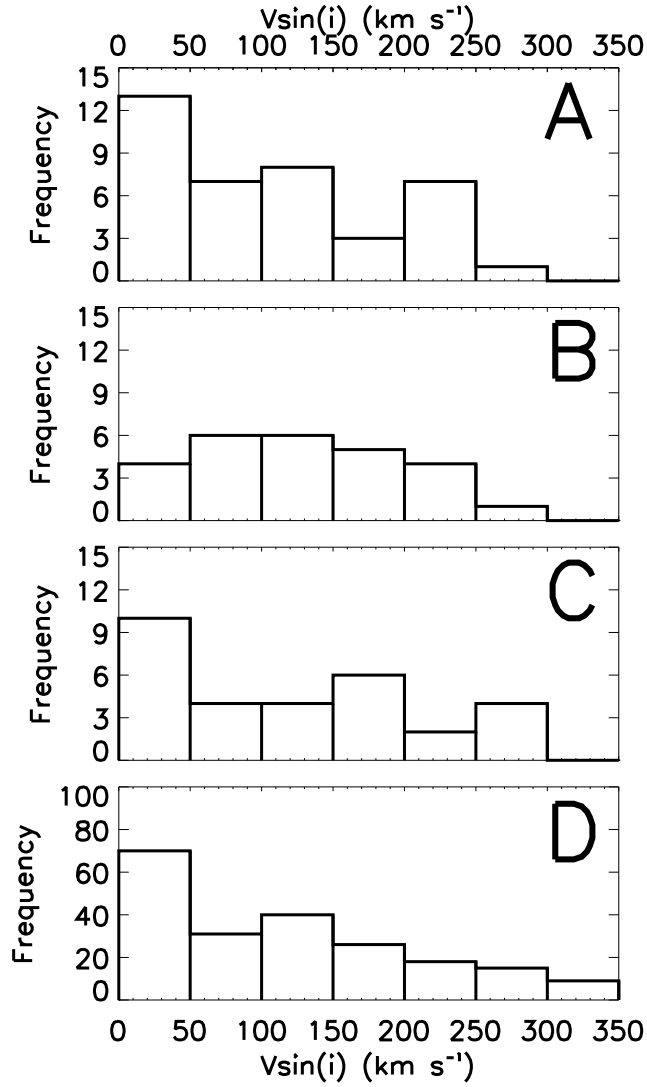


Fig. 10.— Histograms of the  $v \sin(i)$  distribution for various samples (bin size of  $50 \text{ km s}^{-1}$ ). Panel A: all high latitude B stars in our sample; Panel B: only runaway stars in our sample. Panel C: high latitude B stars from Magee et al. (1998); Panel D: B stars in the nearby field from Wolff et al. (1982).

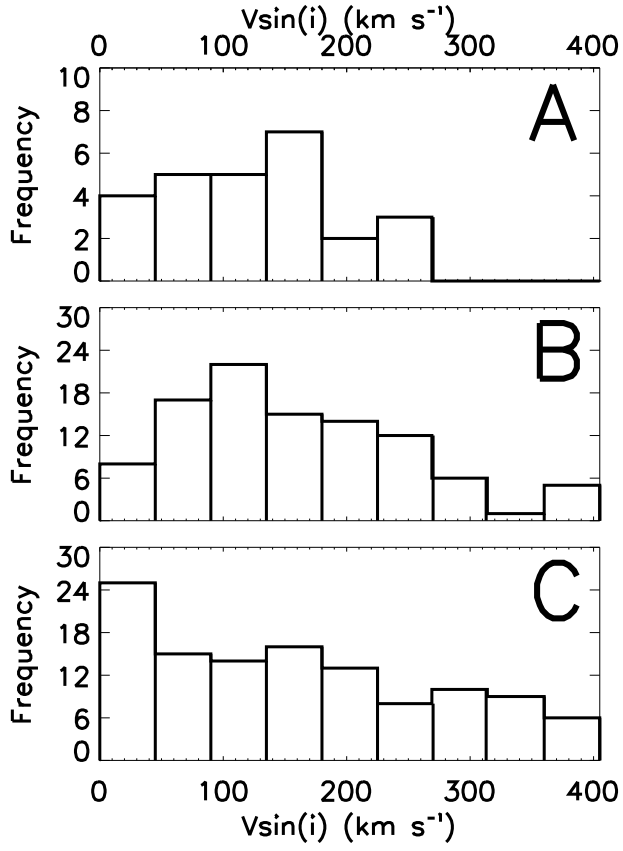


Fig. 11.— Histograms of the  $v \sin(i)$  distribution for various samples (bin size of  $45 \text{ km s}^{-1}$ ). Panel A: runaway stars in our sample. Panel B: “young” OB associations from Guthrie (1984); Panel C: B stars in the nearby field from Guthrie (1984).

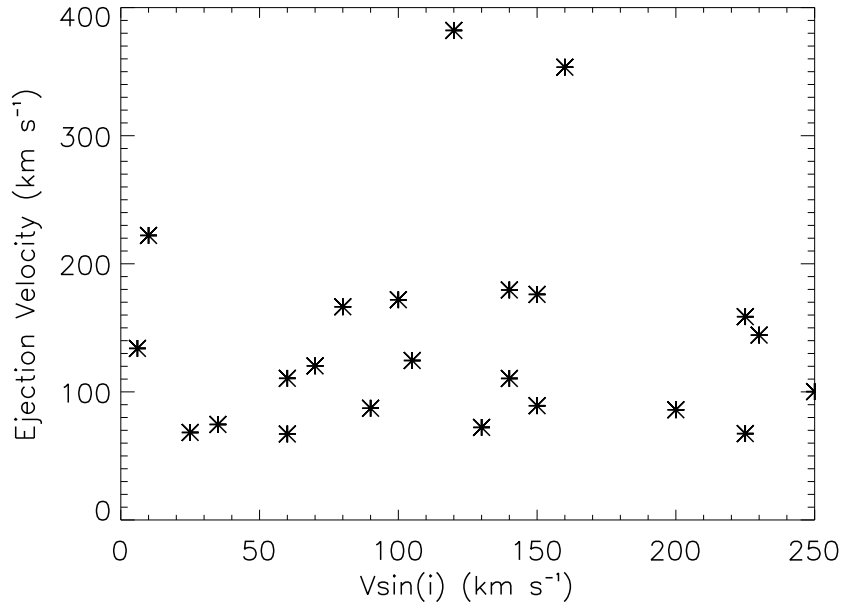


Fig. 12.—  $V \sin(i)$  versus full ejection velocity ( $V_{ej}$ ) for runaway stars in the sample

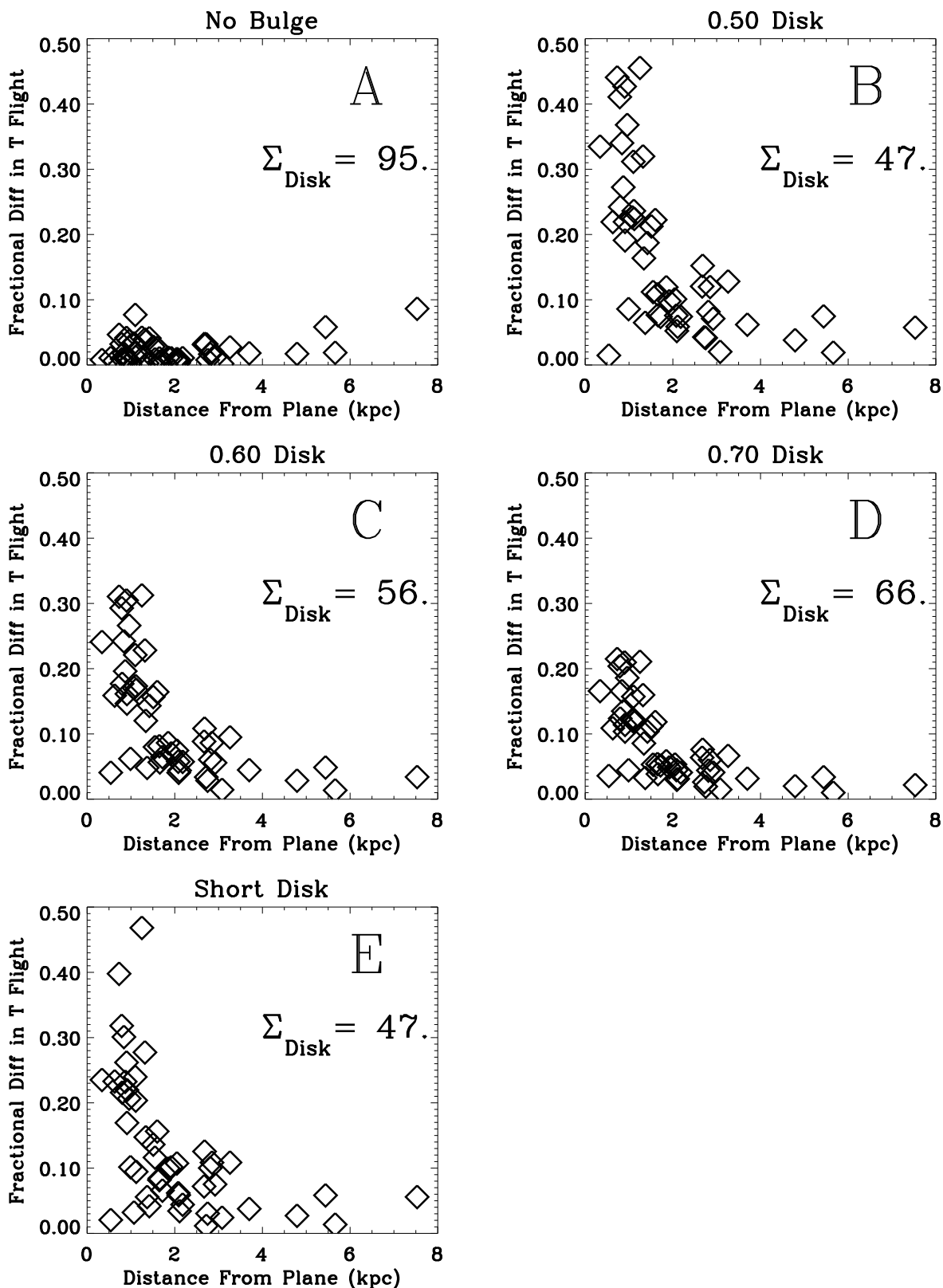


Fig. 13.— Panels A through E show the fractional difference of the flight times for each model described in Table 12 relative to the baseline model as a function of the star’s distance from the galactic plane.



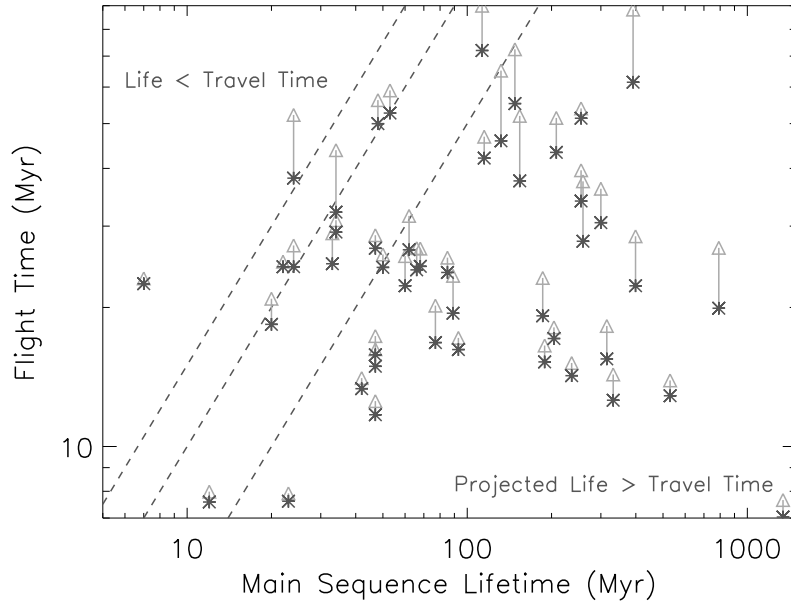


Fig. 14.— The flight time of the star versus its estimated main sequence lifetime. An asterisk (\*) denotes the flight time calculated with the galactic potential model parameters in Table 10. The triangles denote the flight time calculated using the 0.5 Disk model (Table 12).

Table 1. Kinematic Parameters of Galactic Stellar Populations

Population	$V_{\theta}$ ( $\text{km s}^{-1}$ )	$\sigma_{\pi}$ ( $\text{km s}^{-1}$ )	$\sigma_{\theta}$ ( $\text{km s}^{-1}$ )	$\sigma_z$ ( $\text{km s}^{-1}$ )
Thin Disk <sup>a</sup>	214	34	21	18
Thick Disk <sup>a</sup>	184	61	58	39
Halo <sup>b</sup>	25	135	105	90

<sup>a</sup>Edvardsson et al. (1993)

<sup>b</sup>Binney & Merrifield (1998)

Table 2. Parameters of Sample Stars

Star	Average Proper Motion		Source <sup>a</sup>	Radial Vel <sup>b</sup>		Apparent V mag	A <sub>V</sub> <sup>c</sup>	MS Mass <sup>d</sup> (M <sub>⊙</sub> )	Absolute V mag <sup>d</sup>	Distance (kpc)
	μ <sub>α</sub> (mas yr <sup>-1</sup> )	μ <sub>δ</sub> (mas yr <sup>-1</sup> )		km s <sup>-1</sup>	N					
HD 1112	57.0±0.5	10.6±0.5	ACT,CMC	-0.3±5.1	3	8.98	0.12	2.1	+0.63	0.44
HIP 1511	-3.8±1.4	-34.4±1.1	CMC	-229.4±2.4	40	11.61	0.2	1.7	-1.12	3.20
BD -15 115	8.0±1.0	0.1±0.6	ACT,UCAC1	91.3±5.7	64	10.87	0.06	6.8	-1.73	3.22
HD 8323	-4.9±0.6	-17.7±0.4	ACT,UCAC1	-7.0±2.4 <sup>g</sup>	...	9.52	0.13	2.7	+0.02	0.75
BD -7 230	13.2±0.6	-1.2±0.8	ACT,UCAC1	-2.3±1.4	77	11.14	0.11	3.5	-2.12	4.27
Feige 23	-17.4±1.5	-12.9±1.5	CMC	0	1	11.08	0.09	2.4	+0.80	1.09
HD 15910	4.8±0.9	-2.4±0.9	ACT,UCAC1	-44.8±6.0	5	10.1	0.07	2.9	+0.32	0.87
HIP 12320	4.9±1.7	-2.4±1.6	CMC	24.1±12.1	2	12.04	0.27	3.7	-0.46	2.80
HD 21305	-1.4±0.7	2.1±0.8	ACT,UCAC1	73.5±6.7	48	10.35	0.03	6.1	-1.59	2.41
HD 21532	8.6±0.7	3.2±0.5	ACT,UCAC1,CMC	27.8±6.4	25	9.94	0	3.4	+0.31	0.84
HD 40267	-4.0±0.7	8.3±0.6	ACT,UCAC1,CMC	53.9±3.1	27	9.83	0.13	6.3	-2.71	3.06
BD +61 996	2.0±1.0	-5.9±0.8	ACT	83.6±10.4	53	9.9	0.15	8.1	-4.28	6.57
HIP 41979	11.7±0.8	-23.4±0.7	ACT	-2.8±2.7	102	11.48	0.11	6.0	+0.05	1.77
HD 233662	2.1±0.7	-9.8±0.7	ACT	36.3±13.6	4	10.01	0.05	6.9	-3.06	4.01
HD 237844	3.5±1.0	-5.5±0.6	ACT	13.6±11.8	12	10.11	0.02	5.9	-2.16	2.94
BD +16 2114	-12.3±0.7	4.3±0.6	ACT	49.0±2.4 <sup>g</sup>	...	9.98	0.14	3.7	-0.12	0.98
BD +38 2182	-6.7±1.3	0.1±0.8	ACT,CMC	84.2±10.5	7	11.25	0.06	6.6	-2.12	4.60
Feige 40	-1.5±0.7	-6.1±0.7	ACT,CMC	71.5±5.7	7	11.19	0.13	3.9	+0.56	1.26
HD 100340	3.6±1.1	11.4±0.9	ACT	254.4±9.1	9	10.12	0.08	10.	-2.06	2.62
HD 103376	8.7±1.0	5.3±0.7	ACT	20.0±1.6	8	10.22	0.03	3.0	+1.11	0.65
HD 105183	-8.3±0.9	-6.0±0.7	ACT,CMC	34.6±5.4	12	11.07	0.12	4.7	-1.47	3.05
HD 106929	-10.4±0.7	-2.5±0.7	ACT	28.3	1	9.84	0.07	3.1	+1.13	0.53
BD +49 2137	-12.1±0.9	4.8±0.7	ACT	115±10 <sup>h</sup>	...	10.66	0.04	3.4	-0.45	1.64
BD +36 2268	-1.3±1.2	1.4±0.9	ACT	29.2±2.4	16	10.48	0.03	6.9	-2.49	3.86
HD 110166	0.0±0.6	-5.0±0.6	ACT,CMC	-48.4±13.2	2	8.79	0.04	4.2	-2.17	1.53
BD +30 2355	-4.2±0.8	-8.4±1.0	ACT	-5.1±7.7	8	10.64	0.08	3.2	-1.49	2.56
PB 166	-26.4±1.5	10.2±1.4	CMC	43.1±1.5	16	12.45	0.03	5.4	+0.39	2.54
Feige 84	-7.6±1.1	-8.7±0.8	ACT	147.9±9.9	12	11.86	0.06	5.1	-0.65	3.09
HD 121968	1.4±0.9	17.8±0.7	ACT	28±2.4 <sup>g</sup>	...	10.26	0.2	7.4	-2.08	2.67
HD 123884	-0.4±0.8	-2.6±0.7	ACT,UCAC1	16.6±2.6	17	9.36	0.27	3.2	-3.55	3.39
HD 125924	4.6±0.9	-11.7±0.7	ACT,CMC	239.0± 2.4 <sup>g</sup>	...	9.68	0.15	6.9	-1.95	1.98
BD +20 3004	-9.9±0.7	5.7±0.6	ACT	27±10 <sup>h</sup>	...	10.15	0.08	3.6	-2.21	2.85
HD 137569	8.5±0.5	-10.5±0.4	ACT,CMC	-45±3 <sup>f</sup>	...	7.95	0.12	4.7	-3.50	1.84
HD 138503	1.8±0.7	-1.3±0.8	ACT,UCAC1	-53.6±1.2 <sup>e</sup>	...	9.1	0.7	8.1	-3.40 <sup>e</sup>	2.29
HD 140543	-3.4±0.7	-2.4±0.6	ACT,UCAC1	-9±5 <sup>h</sup>	...	8.88	0.84	22	-6.25	7.22
BD +33 2642	-12.7±1.1	1.6±1.0	ACT	-92.3± 2.1	26	10.84	0.04	10.	-4.25	10.24
HD 146813	0.2±0.7	-3.8±0.6	ACT	19.1±5.7	34	9.06	0.03	8.2	-2.58	2.10
HD 149363	-7.6±0.9	-12.8±0.6	ACT	145.8±7.1	49	7.79	0.87	15.	-3.49	1.21
BD +13 3224	-4.6±1.0	3.3±0.6	ACT	2.42±0.53 <sup>i</sup>	...	10.53	0.18	6.9	-1.94	2.88
HD 183899	1.7±0.7	-0.2±0.6	ACT,UCAC1,CMC	-51.3±6.0	28	11.	0.56	9.5	-3.83	4.11
HD 188618	-3.4±0.7	3.5±0.4	ACT,UCAC1	29.0±5.6	12	9.38	0.79	9.7	-3.67	2.83
AG +03 2773	4.2±0.8	-7.3±0.7	ACT	15.6±13.2	24	10.51	0.21	1.6	+2.44	0.40
HD 206144	-6.4±0.8	-11.0±0.6	ACT,UCAC1,CMC	116.7±8.1	21	9.33	0.24	9.7	-3.59	3.52
HD 209684	0.7±0.7	-0.5±0.5	ACT,UCAC1	71.6±7.7	28	9.86	0.12	6.8	-1.23	1.56
HD 213781	-0.5±0.6	3.6±0.5	ACT,UCAC1,CMC	-32.7±6.1	17	9.04	0.19	4.1	-1.18	1.01
HD 216135	-18.5±0.7	-13.8±0.6	ACT,UCAC1	14.5±4.1	11	10.13	0.14	4.5	-0.89	1.49
HD 218970	46.5±0.8	33.4±0.7	ACT,UCAC1,CMC	93.8±4.5	11	9.75	0.08	5.2	-0.71	1.19
HD 220787	3.5±0.7	-1.4±0.5	ACT,UCAC1,CMC	26.4±2.6	18	8.3	0.09	5.7	-1.35	0.82
HD 222040	23.6±1.2	-26.9±0.9	ACT,UCAC1	75.8±1.5	22	10.87	0.08	1.1	+0.23	1.30

<sup>a</sup>Sources averaged into the proper motion in addition to HIP and Tycho-2.

<sup>b</sup>Unless otherwise noted the radial velocity is measured from the spectra. N is the number of independent line measures that went into the radial velocity

<sup>c</sup>See Paper I for details on A<sub>V</sub>.

<sup>d</sup>Absolute magnitude obtained from Schaller et al. (1992) using T<sub>e</sub>ff, log(g), and [Fe/H] assuming that the star is on the hydrogen burning main sequence with bolometric correction from ATLAS12 (Kurucz 1996).

<sup>e</sup>Radial velocity and absolute magnitude from Martin (2003).

<sup>f</sup>Radial velocity from Bolton & Thomson (1980).

<sup>g</sup>Radial velocity from Greenstein & Sargent (1974).

<sup>h</sup>Radial velocity from Evans (1967).

<sup>i</sup>Radial velocity from Lynas-Gray et al. (1984).

Table 3. Radial Velocity Standards

Star	Apparent V Mag	Spectral Class	$v\sin(i)^a$ $\text{km s}^{-1}$	Standard $RV^a$ $\text{km s}^{-1}$	Measured $RV$ $\text{km s}^{-1}$	$N^b$
HR 675	5.03	A2 V	18	$0.43 \pm 0.05$	$0.3 \pm 0.5$	277
HR 1389	4.29	A2 IV-V	8	$38.97 \pm 0.12$	$38.9 \pm 1.0$	75
HR 1397	6.06	B6 IV	25	$12.04 \pm 1.00$	$11.8 \pm 1.5$	151
HR 2010	4.91	B9.5 V	21	$20.55 \pm 0.12$	$19.3 \pm 1.2$	235
HR 2238	4.48	A1 V	41	$-2.01 \pm 0.95$	$-2.1 \pm 0.1$	426
HR 2489	6.46	A9 III	8	$7.68 \pm 0.07$	$8.9 \pm 0.7$	68
HR 2818	4.64	A0 IV	14	$26.81 \pm 0.15$	$27.4 \pm 0.4$	527
HR 3136	5.65	A1 V	29	$44.22 \pm 0.26$	$44.1 \pm 0.1$	492
HR 3383	5.81	A1 V	4	$2.79 \pm 0.09$	$3.7 \pm 0.3$	393
HR 4033	3.45	A1 IV	44	$18.08 \pm 1.03$	$18.9 \pm 0.8$	61
HR 4187	5.80	A0 V	14	$-15.45 \pm 0.93$	$-17 \pm 1.3$	61
HR 4359	3.34	A2 IV	18	$7.44 \pm 0.16$	$7.6 \pm 0.5$	276
HR 7773	4.76	B9.5 V	18	$-1.02 \pm 0.24$	$-1.1 \pm 0.7$	435
HR 8404	5.80	B9.5 V	4	$0.20 \pm 0.05$	$-0.1 \pm 0.3$	615
HR 8768	6.39	B2 V	10	$-11.37 \pm 0.80$	$-10.8 \pm 1.8$	52

<sup>a</sup>Standard radial velocity and  $V\sin(i)$  taken from Fekel (1999).

<sup>b</sup> $N$  is the number of independent line measures averaged in the measured radial velocity.

Table 4. Radial Velocities Versus Published Values

Star	Radial Velocity (km s <sup>-1</sup> )		Reference
	This Work	Literature	
HD 1112	-0.3±5.1	6.0±2.4	Greenstein & Sargent (1974)
...	...	-9.4±9.7	Behr (2003)
BD -15 115	91.3±5.7	86.7	Graham & Slettebak (1973)
...	...	93.0±4.0	Ramspeck et al. (2001b)
...	...	94.0	Conlon et al. (1992)
BD -7 230	-2.3±1.4	2.0±2.4	Greenstein & Sargent (1974)
...	...	-1.7±0.8	Behr (2003)
Feige 23	0.0±10.0 <sup>a</sup>	6.0±2.4	Greenstein & Sargent (1974)
HD 15910	-44.8±6.0 <sup>b</sup>	-79.0±13.0	Harding et al. (1971)
HIP 12320	24.1±12.1 <sup>a</sup>	-5.0±22.0	Greenstein & Sargent (1974)
HD 21532	27.8±6.4	22.0±2.4	Greenstein & Sargent (1974)
HD 233662	36.3±13.6 <sup>b</sup>	11.0	Duflot et al. (1998)
...	...	31.8±22.3	Behr (2003)
BD +38 2182	84.2±10.5	79.0±22.0	Greenstein & Sargent (1974)
Feige 40	71.6±5.7	130.0±26.0	Greenstein & Sargent (1974)
...	...	74.2±14.0	Behr (2003)
HD 100340	254.4±9.1	248.0±22.0	Greenstein & Sargent (1974)
...	...	250.0	Keenan et al. (1987)
...	...	246.0±5.0	Ryans et al. (1999)
...	...	256.9±19.9	Behr (2003)
HD 103376	24.1±1.6	18.0	Duflot et al. (1998)
...	...	7.9±17.6	Behr (2003)
HD 105183	34.6±5.4	34.0±2.4	Greenstein & Sargent (1974)
...	...	22.0	Duflot et al. (1993)
...	...	32.6±15.3	Behr (2003)
HD 106929	28.3±10.0 <sup>a</sup>	16.6±3.7	Grenier et al. (1999)
BD +36 2268	29.2±2.4	31.0	Duflot et al. (1998)
...	...	41.0±5.9	Behr (2003)
HD 110166	-48.4±13.2 <sup>b</sup>	-89.9±2.6	Barbier-Brossat & Figon (2000)
BD +30 2355	-5.1±7.7	-12.0±2.4	Greenstein & Sargent (1974)
...	...	1.2±25.0	Behr (2003)
PB 166	43.1±1.5	60.0	Conlon (1989a)
...	...	43.0	de Boer et al. (1988)
Feige 84	147.9±9.9	148.0±26.0	Greenstein & Sargent (1974)
...	...	153.0±27.8	Behr (2003)
HD 123884	16.6±2.6	6.6	Duflot et al. (1998)
BD +33 2643	-92.3±2.1	-100.0±2.4	Greenstein & Sargent (1974)
...	...	-94.0	Napiwotzki, Herrmann, Heber, & Altmann (2001)
...	...	-94.0±2.5	Behr (2003)
HD 146813	19.1±5.7	21.0±5.0	Grenier et al. (1999)
HD 149363	145.8±7.2	141.4±2.0	Barbier-Brossat & Figon (2000)
HD 183899	-51.3±6.0	-45.0	Duflot et al. (1998)
HD 188618	29.0±5.6	-15.0	Duflot et al. (1998)
HD 206144	116.7±8.1	112.0±11.3	Kilkenny & Hill (1975)
HD 213781	-32.7±6.1	-31.0±2.2	Greenstein & Sargent (1974)
...	...	-30.0±3.5	Behr (2003)
HD 216135	14.5±4.1	-17.0±2.4	Greenstein & Sargent (1974)
HD 218970	93.8±4.5	98.0±2.4	Greenstein & Sargent (1974)
HD 220787	26.4±2.6	24.9±1.5	Barbier-Brossat & Figon (2000)
...	...	26.5±2.4	Behr (2003)
HD 222040	75.8±1.4	65.0±9.0	Harding et al. (1971)

<sup>a</sup>Only Hydrogen Balmer lines were used to measure this radial velocity.

<sup>b</sup>Only Hydrogen Balmer and He I lines were used to measure this radial velocity.

Table 5. Data for Sample Stars

Star	R (kpc)	Position <sup>a</sup>		Velocity (km s <sup>-1</sup> ) <sup>b</sup>			MS Mass <sup>e</sup> M <sub>⊙</sub>	MS Lifetime <sup>e</sup> Myr	T <sub>flight</sub> Myr	Z <sub>ej</sub> (km s <sup>-1</sup> )
		θ (deg) <sup>c</sup>	Z (kpc) <sup>d</sup>	V <sub>π</sub>	V <sub>θ</sub>	V <sub>Z</sub>				
HD 1112	8.2	3.5	-0.3	104±21	188±8	6±3	2.1	800	20±1	-33±2
HIP 1511	9.8	19.7	-1.7	-263±42	-167±33	-301±104	1.7	1300	7±13	-311±100
BD -15 115	9.5	26.7	-3.1	49±19	178±15	-88±5	6.8	50	24±1	-173±6
HD 8323	8.6	3.9	-0.7	-58±8	192±7	-10±6	2.7	400	22±2	-47±2
BD -7 230	11.8	15.8	-3.9	146±34	89±30	37±8	3.5	250	51±4	-313±45
Feige 23	9.1	2.1	-0.9	-73±17	249±5	-60±18	2.4	530	13±3	-79±14
HD 15910	8.8	-2.9	-0.8	5±2	219±4	54±5	2.9	400	61±4	-69±4
HIP 12320	10.7	4.7	-2.1	53±14	185±21	-2±14	3.7	200	43±6	-97±8
HD 21305	10.2	-8.9	-2.0	-0±5	239±7	-57±6	6.1	70	24±1	-98±4
HD 21532	8.7	-3.8	-0.7	40±5	214±3	6±7	3.4	250	28±3	-49±2
HD 40267	10.3	-13.5	-1.1	168±20	298±20	-21±8	6.3	60	27±3	-60±5
BD +61 996	14.2	9.5	3.3	36±24	118±30	95±25	8.1	30	29±5	138±17
HIP 41979	9.6	-3.7	0.9	-118±20	29±38	26±7	6.0	60	22±3	54±4
HD 233662	12.0	2.8	2.8	6±7	45±30	83±16	6.9	50	27±3	123±11
HD 237844	10.8	3.9	2.2	8±10	171±14	68±16	5.9	70	25±4	105±10
BD +16 2114	8.7	-2.6	0.8	61±10	214±2	21±7	3.7	200	19±2	58±2
BD +38 2182	12.6	-0.4	4.1	130±31	242±16	15±21	6.6	50	53±8	147±12
Feige 40	8.6	-3.4	1.1	-5±3	177±7	58±5	3.9	200	15±1	88±4
HD 100340	8.9	-8.0	2.3	16±9	219±24	297±18	10.	20	8±1	313±17
HD 103376	8.3	-1.1	0.6	-19±3	256±5	39±2	3.0	300	13±1	59±2
HD 105183	8.7	-6.4	2.9	50±14	94±24	-4±12	4.7	100	42±3	157±15
HD 106929	8.0	-1.2	0.5	1±3	211±3	17±3	3.1	300	15±1	45±1
BD +49 2137	9.2	2.8	1.5	119±20	267±6	90±9	3.4	250	14±1	121±7
BD +36 2268	11.6	1.6	3.8	66±10	167±24	29±4	6.9	50	50±2	112±5
HD 110166	9.2	1.2	1.5	-43±5	207±7	-34±11	4.2	150	55±6	80±5
BD +30 2355	8.0	13.7	1.7	-36±6	93±19	9±3	3.2	300	31±1	99±2
PB 166	9.2	5.9	2.3	292±56	98±20	41±6	5.4	90	24±2	186±28
Feige 84	5.1	-3.2	3.0	-51±14	34±31	137±9	5.1	90	16±1	218±7
HD 121968	5.7	-6.6	2.2	86±19	416±36	139±28	7.4	40	13±2	191±22
HD 123884	5.4	-14.4	2.2	3±5	151±16	-9±10	3.2	250	34±4	123±9
HD 125924	6.2	-4.5	1.5	-227±14	125±10	108±19	6.9	50	12±2	141±16
BD +20 3004	5.4	4.8	2.6	115±26	205±8	98±18	3.6	200	17±2	199±11
HD 137569	6.3	3.8	1.4	-85±16	169±9	-102±16	4.7	100	72±11	117±11
HD 138503	5.8	-5.9	1.0	12±4	243±5	-35±8	8.1	30	32±4	81±5
HD 140543	1.8	-50.03	3.1	51±12	106±34	19±17	22.	7	23±3	260±44
BD +33 2642	8.3	128.12	7.9	293±76	107±57	327±97	10.	20	24±11	368±91
HD 146813	8.1	10.7	1.5	-5±7	206±12	27±5	8.2	30	25±1	84±2
HD 149363	6.8	1.6	0.5	-141±5	189±16	67±4	15.	10	8±1	82±4
BD +13 3224	5.7	12.6	1.6	104±8	186±11	72±17	6.9	50	15±2	139±11
HD 183899	4.1	13.9	-1.4	-3±6	244±7	-5±13	11.	20	18±3	-146±29
HD 188618	5.5	12.6	-1.1	-88±5	287±8	53±15	9.7	25	38±8	-88±8
AC +03 2773	7.77	2.68	-0.2	-17±4	232±6	-13±6	1.6	4300	13±3	-186±24
HD 206144	5.5	26.7	-2.5	-138±29	94±24	-52±10	9.7	25	25±2	-135±11
HD 209684	7.0	11.2	-1.2	-65±3	274±4	-51±5	6.8	50	16±1	-95±3
HD 213781	7.4	7.9	-0.8	9±2	233±3	40±4	4.1	150	38±2	-76±3
HD 216135	7.2	12.6	-1.3	-200±30	170±11	27±9	4.5	130	46±6	-64±7
HD 218970	7.2	8.8	-1.1	322±64	342±5	-8±10	5.2	90	19±2	-106±7
HD 220787	7.7	7.6	-0.7	-5±2	233±2	-23±2	5.7	80	17±1	-60±1
HD 222040	7.2	10.7	-1.2	23±11	46±36	-127±15	1.1	4600	9±1	-151±12

<sup>a</sup>Assumes that the Sun is 8.0 kpc from the galactic center and 0.0 kpc from the galactic plane.

<sup>b</sup>The velocity of the Sun in this frame is: (V<sub>π</sub>, V<sub>θ</sub>, V<sub>Z</sub>) = (-9 km s<sup>-1</sup>, 232 km s<sup>-1</sup>, 7 km s<sup>-1</sup>)

<sup>c</sup>The angle of separation between the Sun and the star as viewed from the galactic center. Positive angles are measured in the direction of galactic rotation.

<sup>d</sup>The distance from the galactic plane to the star in the direction of the north galactic pole.

<sup>e</sup>Assuming the star is on the hydrogen burning main sequence. Obtained from the tables of Schaller et al. (1992) using T<sub>eff</sub>, log(g), and [Fe/H].

<sup>f</sup>AG +03 2773 is probably an F dwarf (see Paper I).

Table 6. Kinematic Scoring & Final Classifications

Star	$(V_{\pi}+V_{\theta})^a$ km s <sup>-1</sup>	$(T_{flight}/T_{MS})$	Kinematic Score <sup>b</sup>	Abundance Class <sup>e</sup>	Other <sup>d</sup>	Verdict <sup>c</sup>
HD 1112	109	0.03	3	?		OES?
HIP 1511	468	0.05	2	MP (-1)		OES
BD -15 115	65	0.49	2	Disk		Pop I
HD 8323	65	0.06	4			Pop I?
BD -7 230	196	0.20	2	MP (-.5)		Pop I?
Feige 23	78	0.02	4		NaD Em; Paper I, Fig. 12	Pop I?
HD 15910	5	0.16	4	MP (-.5)		Pop I
HIP 12320	63	0.21	4	Disk?		Pop I
HD 21305	19	0.37	4	OES		OES
HD 21532	41	0.11	4	Disk		Pop I
HD 40267	185	0.43	2	OES		OES
BD +61 996	108	0.86	2	Disk?		Pop I
HIP 41979	225	0.37	2	OES	He EW; Paper I, Fig. 11	OES
HD 233662	175	0.58	1	OES?		OES?
HD 237844	50	0.36	4	MP (-.75)		OES?
BD +16 2114	61	0.10	4		ER Leo	Pop I?
BD +38 2182	132	0.99	2	Disk?		Pop I?
Feige 40	44	0.08	4	Disk?		Pop I
HD 100340	16	0.34	4	Disk?		Pop I?
HD 103376	41	0.04	4	Disk?		Pop I
HD 105183	136	0.37	3	OES		OES
HD 106929	9	0.05	4	MP (-.5)		Pop I
BD +49 2137	12	0.06	3			Pop I?
BD +36 2268	84	1.04	3	OES		OES
HD 110166	45	0.37	4	MP (-.5)		Pop I?
BD +30 2355	132	0.10	3	Disk?		Pop I
PB 166	317	0.28	1	OES		OES
Feige 84	193	0.17	2	Disk?		Pop I?
HD 121968	214	0.32	2			U
HD 123884	69	0.13	4	MP (-.75)	Bidelman (1988)	OES?
HD 125924	246	0.25	2			U
BD +20 3004	116	0.08	3			Pop I?
HD 137569	99	0.64	3	OES?	RV Var; Bolton & Thomson (1980)	OES
HD 138503	26	1.00	3	Disk	IT Lib; Martin (2003)	Pop I
HD 140543	125	3.08	1	Disk?		Pop I?
BD +33 2642	314	1.10	1	OES?	PN Em; Paper I, Appendix A	OES
HD 146813	15	0.75	3	Disk		Pop I
HD 149363	144	0.65	2	Disk		Pop I?
BD +13 3224	109	0.32	3		V652 Her; Saio & Jeffery (2000)	OES
HD 183899	24	0.91	3	Disk		Pop I
HD 188618	110	1.58	3	Disk		Pop I
AG +03 2773	40	0.00	4			F Dwarf
HD 206144	187	1.02	1	Disk		Pop I?
HD 209684	85	0.34	4	Disk?		Pop I
HD 213781	16	0.24	4	Disk?		Pop I
HD 216135	206	0.35	2	Disk?		Pop I?
HD 218970	344	0.22	2	Disk?		Pop I?
HD 220787	14	0.22	4	Disk		Pop I
HD 222040	1752	0.00	2	MP (-1.8)		OES?

<sup>a</sup>Distance from  $(V_{\pi}, V_{\theta}) = (0 \text{ km s}^{-1}, 220 \text{ km s}^{-1})$  in the  $V_{\pi}$  versus  $V_{\theta}$  plane.

<sup>b</sup>See text for explanation of scoring.

<sup>c</sup>“Pop I” denotes a massive young Population I star ejected from the galactic disk. “OES” denotes an older evolved star. “U” denotes uncertain, there is not enough information to fit the star into the other two categories. A question mark (?) denotes uncertainty in the classification.

<sup>d</sup>Notes of other factors that were taken into account in the classification, i.e. emission features, strong He I features, or a variable radial velocity (See Paper I).

<sup>e</sup>See Paper I. Blank denotes no abundance data. “Disk” are abundances consistent with the nearby B stars. “MP” are metal poor abundances that are uniformly depressed without measured abundances for key elements that might show that the star is evolved. “OES” are abundances consistent with patterns expected in older evolved stars.

Table 7. Classification of Old Evolved Stars

Star	Abundance Comments <sup>a</sup>	Kinematic Score	Log( $T_{eff}$ ) <sup>a</sup>	Log( $g$ ) <sup>a</sup>	Near HB?	$v_{sin(i)}$ (km s <sup>-1</sup> )	$v_{crit}$ <sup>6</sup> (km s <sup>-1</sup> )	Class
HD 1112	Al, Si, Fe only, don't agree	3	4.06	4.00	Yes	130	290	Ambiguous?
HIP 1511	Fe peak only =-1.3	2	3.95	3.00	Yes	20	170	HB
HD 21305	Partial CNO pattern, atomic diffusion	4	4.27	4.00	No	15	290	HB
HD 40267	NO up, C down	4	4.23	3.50	No	100	220	Ambiguous
HIP 41979	Partial CNO pattern?, atomic diffusion	1	4.25	4.50	Yes	8	380	HB
HD 233622	O up?; Z ~ -0.75	1	4.32	3.50	No	225	220	Ambiguous?
HD 237844	Z ~ -0.75	4	4.30	3.75	No	225	250	Ambiguous?
HD 105183	N up, C down	3	4.18	3.75	No	70	250	Ambiguous
BD +36 2268	N up, C down, Si + Al low	3	4.30	3.75	No	60	250	Ambiguous
PB 166	Partial CNO pattern, atomic diffusion	0	4.30	4.75	Yes	5	440	HB
HD 123884	Z ~ -0.75 and Bidelman (1988)	4	4.05	2.5	No	20	120	Post-HB?
HD 137569	C down, S (-.41)	3	4.09	2.75	No	20	140	Post-HB
BD +33 2642	Al low, S + Ar (-.5), C up, N + O up?	1	4.33	3.25	No	5	190	Post-HB
BD +13 3224	Spectra not analyzed	3	4.45	4.00	No	narrow	290	He-Rich Pulsator <sup>b</sup>
HD 222040	Fe peak only =-1.8	2	3.91	3.25	Yes	6	200	HB?

<sup>a</sup>Data from Paper I.

<sup>b</sup>See Saio & Jeffery (2000).

<sup>c</sup>The critical rotational velocity for an evolved star of this mass and surface gravity. See text.

Table 8. Sample Breakdown Compared With Others

	Total	Pop I(%)	OES(%)	Unknown
This Study <sup>a</sup>	48	31(64%)	15(31%)	2(4%)
G&S Stars <sup>b</sup>	32	23(72%)	7(25%)	2(6%)
Magee et al. (2001)	21	14(67%)	7(33%)	...
Rolleston et al. (1997)	25	17(68%)	7(28%)	...
Ramspeck et al. <sup>c</sup>	18	14(78%)	4(22%)	...

<sup>a</sup>The F dwarf AG +03 2773 has been dropped from the sample in this table.

<sup>b</sup>The stars in our sample taken from Greenstein & Sargent (1974).

<sup>c</sup>Numbers combined from Ramspeck et al. (2001a) and Ramspeck et al. (2001b).



Table 9. Revised OES Distances And Velocities

Star	Model <sup>a</sup>	Mass (M <sub>⊙</sub> ) <sup>a</sup>	M <sub>V</sub> <sup>a</sup>	D (kpc)	V <sub>π</sub> (km s <sup>-1</sup> )	V <sub>θ</sub> (km s <sup>-1</sup> )	V <sub>z</sub> (km s <sup>-1</sup> )
BHB Stars							
HIP 1511	e64	0.56	0.22	1.73±0.52	-200±23	-61±18	-103±56
HD 21305	z62	0.52	1.52	0.57±0.17	22±2	217±2	-54±4
HIP 41979	z22	0.49	3.05	0.46±0.14	-42±5	182±9	11±2
PB 166	z22	0.49	3.07	0.74±0.22	94±17	209±6	45±2
HD 222040	g14	0.64	0.61	1.09±0.33	13±9	77±31	-117±13
Post-HB Stars							
HD 123884	e64	0.51	-1.79	1.50±0.45	-10±2	194±6	6±5
HD 137569	j63	0.52	-1.83	0.85±0.26	-31±8	200±3	-67±7
BD +33 2642	...	...	...	3.30±0.40 <sup>b</sup>	101±11	90±11	62±15
BD +13 3224	...	...	...	1.70±0.02 <sup>c</sup>	60±2	212±3	46±5
Ambiguous							
HD 1112	e64	0.56	+1.51	0.30±0.09	67±14	202±6	6±3
...	...	2.1	+0.63	0.44±0.13	104±21	188±8	6±3
HD 40267	z42	0.51	-0.94	1.34±0.40	84±8	243±8	-16±3
...	...	6.3	-2.71	3.06±0.92	168±20	298±20	-21±8
HD 233662	e64	0.52	-0.21	1.08±0.32	15±6	181±9	46±8
...	...	6.9	-3.06	4.01±1.20	6±7	45±30	83±16
HD 237844	e64	0.51	+0.43	0.85±0.26	6±5	216±4	32±8
...	...	5.9	-2.16	2.94±0.88	8±10	171±14	68±16
HD 105183	z22	0.49	+1.07	0.95±0.28	9±4	181±7	26±5
...	...	4.7	-1.47	3.05±0.92	50±14	94±24	-4±12
BD +36 2268	e64	0.51	+0.38	1.03±0.31	15±3	223±4	34±2
...	...	6.9	-2.49	3.86±1.16	66±10	167±24	29±4

<sup>a</sup>From tracks of Dorman et al. (1993) for the following model series: g14 ( $Y_{HB} = 0.245$ ;  $[\text{Fe}/\text{H}] = -2.26$ ), e64 ( $Y_{HB} = 0.247$ ;  $[\text{Fe}/\text{H}] = -1.48$ ), j63 ( $Y_{HB} = 0.257$ ;  $[\text{Fe}/\text{H}] = -0.47$ ), z22 ( $Y_{HB} = 0.288$ ;  $[\text{Fe}/\text{H}] = +0.00$ ), z42 ( $Y_{HB} = 0.292$ ;  $[\text{Fe}/\text{H}] = +0.39$ ), z62 ( $Y_{HB} = 0.289$ ;  $[\text{Fe}/\text{H}] = +0.58$ ).

<sup>b</sup>Distance taken from Napiwotzki, Heber, & Koeppen (1994).

<sup>c</sup>Distance taken from Jeffery et al. (2001).

Table 10. Galactic Potential Model Parameters

Miyamoto & Nagai (1975) Disk Potential	
$\Phi_{disk} = -\frac{GM_{disk}}{\sqrt{R^2 + (a + \sqrt{z^2 + b^2})^2}}$ $M_{disk} = 1.0 \times 10^{11} M_{\odot}$ $a = 6.5 \text{ kpc}$ $b = 0.26 \text{ kpc}$	
Hernquist (1990) Bulge/Spheroidal Potential	
$\Phi_{spheroid} = -\frac{GM_{bulge}}{r+c}$ $M_{bulge} = 3.4 \times 10^{10} M_{\odot}$ $c = 0.7 \text{ kpc}$ $r = \sqrt{R^2 + z^2}$	
Dark Halo Logarithmic Potential	
$\Phi_{halo} = -(v_{halo})^2 \times \ln(r^2 + d^2)$ $v_{halo} = 128 \text{ km s}^{-1}$ $d = 12.0 \text{ kpc}$	

Table 11. Comparison with Magee et al. (2001)

Star	Flight Time (Myr)		Ejection Velocity (km s <sup>-1</sup> )	
	Magee	This Work	Magee	This Work
EC 00321-6320	30	45±3	58	57±2
EC 00358-1516	32	29±1	278	226±18
EC 00468-5622	33	39±2	93	96±3
EC 03342-5243	17	18±1	145	89±3
EC 05515-6231	21	36±4	37	39±4
EC 19071-7634	6	6±1	266	178±31
EC 19337-6734	23	14±2	48	39±3
EC 19476-4109	52	35±6	79	81±9
EC 20089-5659	35	21±3	60	39±2

Table 12. Alternate Galactic Potential Models

Model	$\Sigma_{disk}$ ( $M_{\odot} \text{ pc}^{-2}$ )	$M_{disk}$ ( $M_{\odot} \times 10^{11}$ )	$a^b$ (kpc)	$M_{bulge}$ ( $M_{\odot} \times 10^{10}$ )	$c^c$ (kpc)	$v_{halo}$ ( $\text{km s}^{-1}$ )	$d^d$ (kpc)
Baseline <sup>a</sup>	95	1.00	6.5	3.4	0.7	128	12.0
(A) No Bulge	95	1.00	6.5	0.0	0.0	103	1.0
(B) Disk 0.5	47	0.50	6.5	3.4	0.7	113	4.0
(C) Disk 0.6	56	0.60	6.5	3.4	0.7	115	5.0
(D) Disk 0.7	66	0.70	6.5	3.4	0.7	115	6.0
(E) Short Disk	47	0.67	2.6	0.0	0.0	132	6.5

<sup>a</sup>The baseline model is the model in Appendix A.

<sup>b</sup>Disk scale length

<sup>c</sup>Bulge scale length

<sup>d</sup>Halo scale length